AD-A076 202 PENNSYLVANIA STATE UNIV UNIVERSITY PARK MATERIALS RE--ETC F/G 20/3
MAGNETOFERROELECTRICS, DIVERTABLE FERROELECTRICS AND PYROELECTR--ETC(U)
JUN 79 R E NEWNHAM , L E CROSS , W A SCHULZE DAAG29-76-G-0145

UNCLASSIFIED ARO-13731.4-P NL

| OF |
ADA
076202

END
DATE
FILMED
12-79
DDC

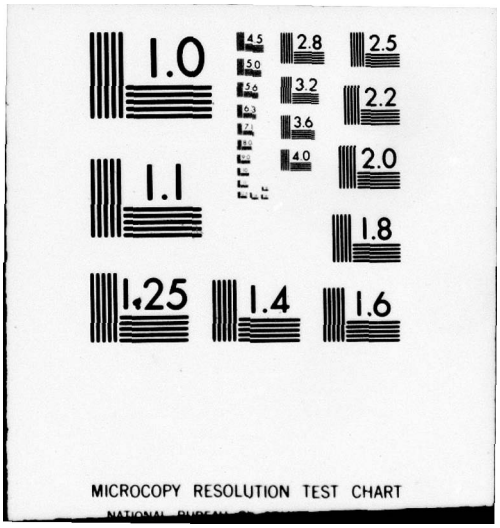
1.0
1.1
1.25
1.4
1.6
1.8
2.0
2.2
2.5
2.8
3.2
3.6
4.0
4.5
5.0
5.6
MICROCOPY RESOLUTION TEST CHART

Magnetoferroelectrics, Divertable Ferroelectrics and Pyroelectric Glass-Ceramics

Final Report

R.E. Newnham, L.E. Cross, W.A. Schulze and A.S. Bhalla

June 21, 1979

U.S. Army Research Office

Contract No. DAAG29-76-G-0145

Materials Research Laboratory
The Pennsylvania State University
University Park, Pennsylvania 16802

Approved for Public Release;
Distribution Unlimited.

MATERIALS RESEARCH LABORATORY
THE PENNSYLVANIA STATE UNIVERSITY
UNIVERSITY PARK, PENNSYLVANIA 16802

The findings in this report are not to be construed as an official Department of the Army position, unless so designated by other authorized documents.

SECURITY CLASSIFICATION OF THIS PAGE (When Data Entered)

REPORT DOCUMENTATION PAGE

READ INSTRUCTIONS BEFORE COMPLETING FORM

1. REPORT NUMBER

2. GOVT ACCESSION NO.

3. RECIPIENT'S CATALOG NUMBER

4. TITLE (and Subtitle)
(6) Magnetoferroelectrics, Divertable Ferroelectrics and Pyroelectric Glass Ceramics.

5. TYPE OF REPORT & PERIOD COVERED
Final

6. PERFORMING ORG. REPORT NUMBER

7. AUTHOR(s)
(10) R.E. Newnham, L.E. Cross, W.A. Schulze, A.S. Bhalla

8. CONTRACT OR GRANT NUMBER(s)
(15) ✓DAAG29-76-G-0145

9. PERFORMING ORGANIZATION NAME AND ADDRESS
Materials Research Laboratory
The Pennsylvania State University
University Park, Pennsylvania 16802
(17) 05

10. PROGRAM ELEMENT, PROJECT, TASK AREA & WORK UNIT NUMBERS
(16) Project No. P13713-P
IT161102BH57-05 Physics

11. CONTROLLING OFFICE NAME AND ADDRESS
U. S. Army Research Office
Post Office Box 12211
Research Triangle Park, NC 27709
(11)

12. REPORT DATE
21 Jun 1979

13. NUMBER OF PAGES

14. MONITORING AGENCY NAME & ADDRESS (if different from Controlling Office)
(18) ARO
(19) 13731.4-P

15. SECURITY CLASS. (of this report)
Unclassified

15a. DECLASSIFICATION/DOWNGRADING SCHEDULE
NA

16. DISTRIBUTION STATEMENT (of this Report)
(12) 66
(9) Approved for public release; distribution unlimited.
Final rept.
22 Mar 76-21 Jun 79,

DDC RECEIVED NOV 7 1979 E

17. DISTRIBUTION STATEMENT (of the abstract entered in Block 20, if different from Report)
NA

18. SUPPLEMENTARY NOTES
The view, opinions, and/or findings contained in this report are those of the author(s) and should not be construed as an official department of the Army position, policy, or decision unless so designated by other documentation.

19. KEY WORDS (Continue on reverse side if necessary and identify by block number)
Magnetoferroelectric, Irreversible Ferroelectrics, Piezoelectrics, Optical Second Harmonic Generation, Crystal Growth.

20. ABSTRACT (Continue on reverse side if necessary and identify by block number)
The highlight of the past three years was the discovery of magnetoferroelectricity, a new type of ferroelectricity caused by the ordering of magnetic spins in a low symmetry arrangement. A magnetoferroelectric develops a reversible spontaneous electric polarization on passing through a magnetic phase transition. The effect was demonstrated on Cr_2BeO_4 which undergoes a phase transformation from a centric paramagnetic state to a complex antiferromagnetic state at 28K. Ceramic specimens can be poled electrically below the →

DD FORM 1 JAN 73 1473 EDITION OF 1 NOV 65 IS OBSOLETE

SECURITY CLASSIFICATION OF THIS PAGE (When Data Entered)

220 750 LB

transition temperature to a remnant polarization about five orders of magnitude smaller than $BaTiO_3$. No dielectric anomaly is observed at T_c, but both the remnant polarization and the pyroelectric coefficient can be reversed in sign with a poling field.

Additional magnetoferroelectric studies have been carried out on single crystals of Cr_2BeO_4 and on certain mixed crystals in the Fe_2O_3-Cr_2O_3 system.

A high-sensitivity optical harmonic system was built and tested on some interesting materials. Second harmonic signals were observed from $PbZrO_3$ ceramics, verifying the acentric nature of this important end member of the PZT system. Signals were also detected from kaolinite, providing the first macroscopic evidence of polarity in the stacking of aluminosilicate layers in a clay mineral.

Divertable ferroelectrics are an interesting group of materials in which the spontaneous polarization can be reoriented, but not reversed. The results of some experiments on nickel iodine boracite, and on barium titanium germanate are described in this report.

Lastly, a new class of pyroelectric materials is reported. Carefully crystallized lithium silicate glass-ceramics are found to be pyroelectric. Oriented $Li_2Si_2O_5$ crystallites give rise to pyroelectric coefficients of the order of 10^{-9} C/cm^{2}K and dielectric constants of 6.0.

Contents

	Page
1. INTRODUCTION	1
2. MAGNETOFERROELECTRICS	3
2.1 Chromium Chrysoberyl Cr_2BeO_4	3
2.2 Cr_2O_3:Fe_2O_3 Solid Solutions	3
3. OPTICAL HARMONIC SIGNALS FROM LAYER SILICATES AND FROM $PbZrO_3$	6
4. DIVERTABLE FERROELECTRICS	8
4.1 Introduction	8
4.2 Barium Titanium Germanate	9
4.2.1 Introduction	9
4.2.2 Crystal Growth	9
4.2.3 Optical Properties	11
4.2.4 Preliminary X-Ray Studies	13
4.2.5 Discussion	14
5. GLASS CERAMIC COMPOSITES	15
Appendix 1 Magnetoferroelectricity in Cr_2BeO_4	
Appendix 2 Crystal Growth of the Corundum-Type Iron and Chromium Oxide Solid Solution by Chemical Transport Reaction	
Appendix 3 Crystal Growth, Characterization and Electrical Properties of Corundum Type $(Cr_{1-x}Fe_x)_2O_3$ Solid Solution	
Appendix 4 Optical Second Harmonic Signals from Clay Minerals	
Appendix 5 Second Harmonic Generation in Antiferroelectric PZT	

1. INTRODUCTION

This report documents work carried out over the period March 22, 1976 to June 21, 1979, in the Materials Research Laboratory of The Pennsylvania State University under Contract No. DAAG29-76-G-0145. Our major accomplishment during the present period has been the discovery of a new class of ferroelectric material possessing a magnetically induced ferroelectricity to which the name "magnetoferroelectric" has been given. This effect was predicted on the basis of symmetry arguments and was experimentally confirmed in chromium chrysoberyl, Cr_2BeO_4, by the observation of reversible pyroelectricity below the Neél temperature in this crystal. A paper describing this work has appeared in the Journal of Applied Physics and is included as Appendix 1 of this report.

Current work on this interesting topic is now concerned with an examination of solid solutions in the Cr_2O_3:Fe_2O_3 system. The symmetry conditions in this system are such that for compositions between 20 and 35 mole% Fe_2O_3 a similar cycloidal magnetic structure occurs but with Neél temperatures between 150 and 300 K. Initial attempts to produce ceramic samples of these compositions were completely frustrated by our inability to find any combination of temperature or pressure conditions under which the powders could be effectively densified. By using chemical transport methods, however, small single crystals in the correct composition range have now been grown and these will be much superior to ceramics for the proper characterization of the magnetoferroelectric parameters, (Appendice 2 &3).

Using the very high sensitivity optical second harmonic generation system which was originally constructed for the magnetoferroelectric studies, we have been able to detect optical harmonic signals from a number of very poorly crystallized clay minerals, and thus to provide new symmetry information of vital interest to the clay mineralogists and petroleum engineers (Appendix 4). Based on these data, sponsorship for an enlarged program of study in this area

has been obtained from the American Chemical Society through the Petroleum Research Fund.

Further tests were performed on several mica specimens, and on antiferroelectric $PbZrO_3$. Centric and acentric mica polytypes can be distinguished in this way. Harmonic signals from orthorhombic $PbZrO_3$ confirm the acentric point group assignment 222. Details are given in appendix 5.

Another major area of study on this contract is concerned with divertable but irreversible ferroelectrics. Studies of the hydrothermal growth of the divertable but irreversible boracites has been discontinued, as this topic has now been taken up by Philips Laboratories with a substantial experimental effort. Present studies are concentrated on the germanium analog of the mineral fresnoite ($Ba_2TiGe_2O_8$). Current work indicates that this may be in the divertable:irreversible species 4mmF1 with a transition to the polar ferroelastic species 4mmF2 at 400°C.

Our most recent investigations concern the development of polar effects in glass ceramics. Oriented crystallites were grown in lithium silicate glass matrices, leading to a new class of pyroelectric materials. These are <u>not</u> ferroelectric glass-ceramics, but ordinary silicate pyroelectrics similar to tourmaline in properties. Further results will be reported in the next contract period.

2. MAGNETOFERROELECTRICS

2.1 Chromium Chrysoberyl Cr_2BeO_4

The successful demonstration of the magnetoferroelectric effect in Cr_2BeO_4 has been written up and published in the Journal of Applied Physics. A copy of this paper is included with the report as Appendix 1. The work reported in that study was carried through on sintered compacts of the chrysoberyl. Some very small single crystals of this material are available from the original neutron diffraction studies of the spin structure[1] and work is now going forward to miniaturize the pyroelectric measuring head so that measurements can be repeated for different orientations in the single crystal.

2.2 Cr_2O_3:Fe_2O_3 Solid Solutions

Solid solutions of chromium and iron oxides are interesting potential candidate materials for the magnetoferroelectric effect. As was documented in an earlier report[2] we hoped to measure this phenomenon using ceramic samples with the required composition in the range 20-35% Fe, which are known to possess magnetic structures of appropriate symmetry but significantly higher Neél temperatures than the chrysoberyl.

It has, however, become clear after an extensive series of attempts, that we are unable to achieve suitable densification with any conditions available in this Laboratory. Attempts at direct sintering in either oxygen or nitrogen atmospheres at temperatures up to 1700°C were not effective. Hot isostatic pressing at temperatures up to 1300°C and pressures of 2500 psi were also of no avail. In view of these difficulties, it was decided to change direction completely and attempt single crystal growth.

For the Cr_2O_3 and Fe_2O_3 there are many papers describing techniques for crystal growth[3-6]. However, in the solid solution family between these end member compositions very little earlier work could be traced. Estimating from the flux growth studies of Berkes[7], it would appear that only some 1% Fe was

incorporated in crystals even when 30 mole% Fe_2O_3 was introduced into the melt. In view of this potentially serious segregation problem, it was decided to concentrate on growth by chemical transport.

In these chemical vapor transport studies, Cl_2 was used as the transporting agent. Since it is rather hazardous to handle Cl_2 gas directly, $FeCl_3$ was used which in reaction with oxygen gas gives the transporting species through the reaction

$$2\ FeCl_3 + 3/2\ O_2 \rightleftharpoons Fe_2O_3 + Cl_2$$

A paper describing crystal growth work (appendix 2) has been submitted for publication in the Journal of Crystal Growth. Same results on the growth and electrical properties of $Fe_{1-x}Cr_xO_3$ crystals are presented in the second European Conference on Crystal Growth, held at Lancaster University, England (Sept. 10 to 15, 1979), Abstract and summary of which is included in appendix 3.

References

1. D.E. Cox, B.C. Fraser and R.E. Newnham, J. Appl. Phys. 40(3) 1124 (1969).
2. Progress Report Contract DAAG-29-76-G-0145, Jan. 1, 1978 to June 30, 1978.
3. A.A. Popova, Rost Kristallov, Vol. 4, p. 148, Izdatel'stvo Akad. Nauk SSSR (1964).
4. P. Peshev, G. Bliznakov, G. Gyurov and M. Ivanova, Mat. Res. Bull. 8, 1011 (1973).
5. I. Sunagawa, Am. Min. 45, 566 (1960).
6. P. Kleiner, Z. anorg. allg. chem. 378, 71 (1970).
7. R.E. Barks, Doctoral Thesis in Geochemistry, The Pennsylvania State University.

3. OPTICAL HARMONIC SIGNALS FROM LAYER SILICATES AND FROM $PbZrO_3$

The detection of optical second harmonic signals from clay minerals, first made during the past contract period, opens up a new field of application for this technique. The information provided by such studies is, of course, of particular interest to clay mineralogists, petroleum engineers, etc., and so sponsorship of the study has been taken over by the American Chemical Society, through the award of a Petroleum Institute Fellowship. No further funds are being requested from AROD.

Briefly, when irradiated with a beam of light from a neodymium glass laser, certain clay minerals produce second harmonic signals strong enough to be detected using time-synchronized pulse detection. In the case of well-crystallized nacrite and dickite samples, the signal strengths are comparable with those from quartz, but signals from poorly-crystallized halloysite and kaolinite are noticeably weaker, indicating a dependence on particle size as well as on the acentricity of the mineral structure. No signal is detected from pyrophyllite, as expected for a centric structure. The work is now being extended to the mica family, since it has been shown possible to distinguish ordered from disordered Al-Si arrangements and hence provide a technique for the rapid screening of micas with respect to their thermal histories. To date, signals have been detected from zinnwaldite, ephesite, and margarite, but not from biotite, lepidolite, muscovite, or phlogopite. A paper, published in "Physics and Chemistry of Minerals", is attached as Appendix 4 to the Report.

The SHG studies have further been extended to solve some of the conflicting views about the polar nature of antiferroelectric $PbZrO_3$. The room temperature SHG studies suggest that the structure of antiferroelectric $PbZrO_3$ is not polar but most likely is acentric. A paper describing this work has been

presented at the American Ceramic Society meeting, Sept. 16-18, 1979, at Williamsburg, Va. and a copy of the manuscript is included as appendix 5 of this report.

4. DIVERTABLE FERROELECTRICS

4.1 Introduction

The possibility of divertable but irreversible ferroelectricity was first predicted some ten years ago by Aizu[1] and Shuvalov[2] from symmetry considerations, but there are still only a few good examples of this phenomenon in known crystals and not much progress has been made in unraveling the interesting domain structures and switching characteristics in these materials.

Schmid and co-workers have made extensive studies of the ferroelectric boracites[3,4] which include the irreversible species $\bar{4}3mF3m$ and $\bar{4}3mFm$. Some studies have been made of domain character and irreversibility in the trigonal boracites, but little is known about the monoclinic species. A major problem with all boracites is that of crystal growth. Most members of the family have been grown by vapor transport, but the resulting crystals are often small, highly sectored, and unsuitable for detailed domain studies. Heretofore, our studies have been concerned with possibilities for hydrothermal growth of boracites, and with a search for new irreversible species.

Since the hydrothermal growth of boracites has now been taken up by Philips Laboratories, with a very substantial experimental effort, we propose to focus future work upon the search for new materials.

Present studies suggest that the fresnoite analog barium titanium germanate ($Ba_2TiGe_2O_8$) may be at room temperature in the divertable:irreversible species 4mmF1. The basis for this expectation will be briefly discussed and the proposed studies required to verify the symmetry and investigate the domain and switching characteristics in this crystal will be described. Crystal chemical considerations suggest that a range of solid substitution may be possible in the fresnoite type structure, and we propose to examine the effects of such modification on the phase stability in the $Ba_2TiGe_2O_8$.

4.2 Barium Titanium Germanate

4.2.1 Introduction

Barium titanium germanate, $Ba_2TiGe_2O_8$, was identified by Masse and Durif[6] and by Blasse[7] as having a structure similar to that of the mineral fresnoite ($Ba_2TiSi_2O_8$) with tetragonal P4bm symmetry. More recently, Kimura et al.[8], from an examination of single crystals grown from stoichiometric melts by a Bridgman technique, have identified a solid state phase transition at ~810°C which, they report, reduces the point symmetry from 4mm to mm2, leading to a mimetically twinned ferroelastic structure (4mmFmm2). Twinning corresponds to an interchange of the a and b axes in the orthorhombic, low temperature phase across the twin boundaries, which are the <110> planes of the high temperature group (90° twins). Lattice constant measurements reveal a peculiar long b-axis spacing, which is reportedly 11 x a_o. In a second paper, Kimura et al.[9] confirm ferroelasticity in the lower temperature phase by observing stress detwinning at 700°C under a uniaxial stress of 100 kg/cm^2, and report some elastic and piezoelectric data for their crystals.

4.2.2 Crystal Growth

Crystals for this study were grown by the Czochralski pulling method from stoichiometric melts using a standard A.D. Little model crystal puller. A thick-walled platinum crucible acted as susceptor, and typical growth conditions are given in Table 2. It has proven difficult to grow large (2cm) diameter boules which are crack-free, and growth studies are continuing. Fortunately, however, sections adequate for optical and x-ray studies could be cut from present boules.

Suitable sections were oriented by a Laue technique, utilizing the pseudo four-fold symmetry of the twinned crystals, and plates with major (001) and (110)

Table 2

GROWTH CONDITIONS FOR SINGLE CRYSTAL $Ba_2Ge_2TiO_8$

Crucible	Platinum
M.P.	1260°C
Pulling atmosphere	Air
Initial pulling rate	10 mm/hr
Final pulling rate	2 mm/hr
Rotation rate	20 rpm
Crystal boule size	8 mm dia x 15 mm length
Temperature gradient above the crucible (for 2 cm)	150°C/cm

faces were cut using an abrasive string saw. After cutting and polishing, orientation was rechecked using the conoscopic figures in polarized light.

4.2.3 Optical Properties

Examination of the 'c' (001) plates in polarized light at room temperature revealed the characteristic 90° twinning observed by Kumura et al.[8]. The virgin crystal sections exhibited both twin components with almost equal area and, as expected, the sign of the birefringence (Δn_{ab}) alternates between major twins. Viewing a restricted area under high magnification in conoscopic illumination showed a characteristic biaxial figure with the 'c' axis as acute bisectrix.

Two features of our crystals are, however, at variance with the assignment to the ferroelastic species 4mmFmm2.

(1) The extinction angles between 90° major twin components differ by 4° at 25°C.

(2) On heating through 400°C, there is an obvious first order phase change which drastically reduces the concentration of major 90° twins.

Over the temperature range from 25°C to 400°C, the extinction angle between twins increases only slowly to 6°, but above 400°C there is a more rapid increase (Figure 4.1) until a second phase change at 806°C which eliminates all twinning. Above 806°C the c-sections show no discernible birefringence in parallel light and a clear uniaxial figure in conoscopic illumination.

Measurements of the birefringence, Δn_{ab}, show a continuous monotonic fall with increasing temperature, and an abrupt first order decrease to zero at 806°C, with no evidence of any major change at 400°C (Figure 4.2).

Examination of several (110) sections in polarized light showed some with twin walls running parallel to c along (001), and perpendicular to the surface. We presume that these are traces of suitable oriented 90° twins emerging from the 110 surface. Again, contrary to expectation from previous work, these twin walls are clearly visible and in parallel polarized light

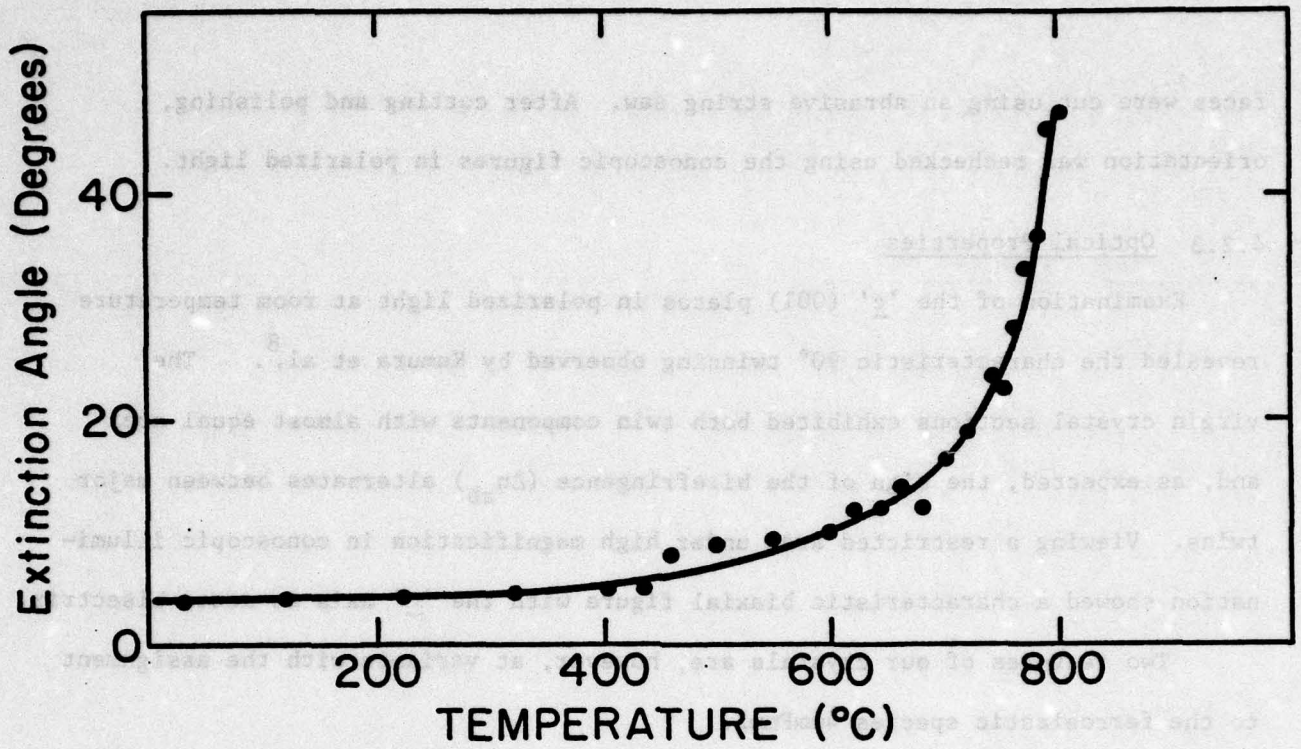

Fig. 4.1 Extinction angle between twins in $Ba_2TiGe_2O_8$ as a function of T.

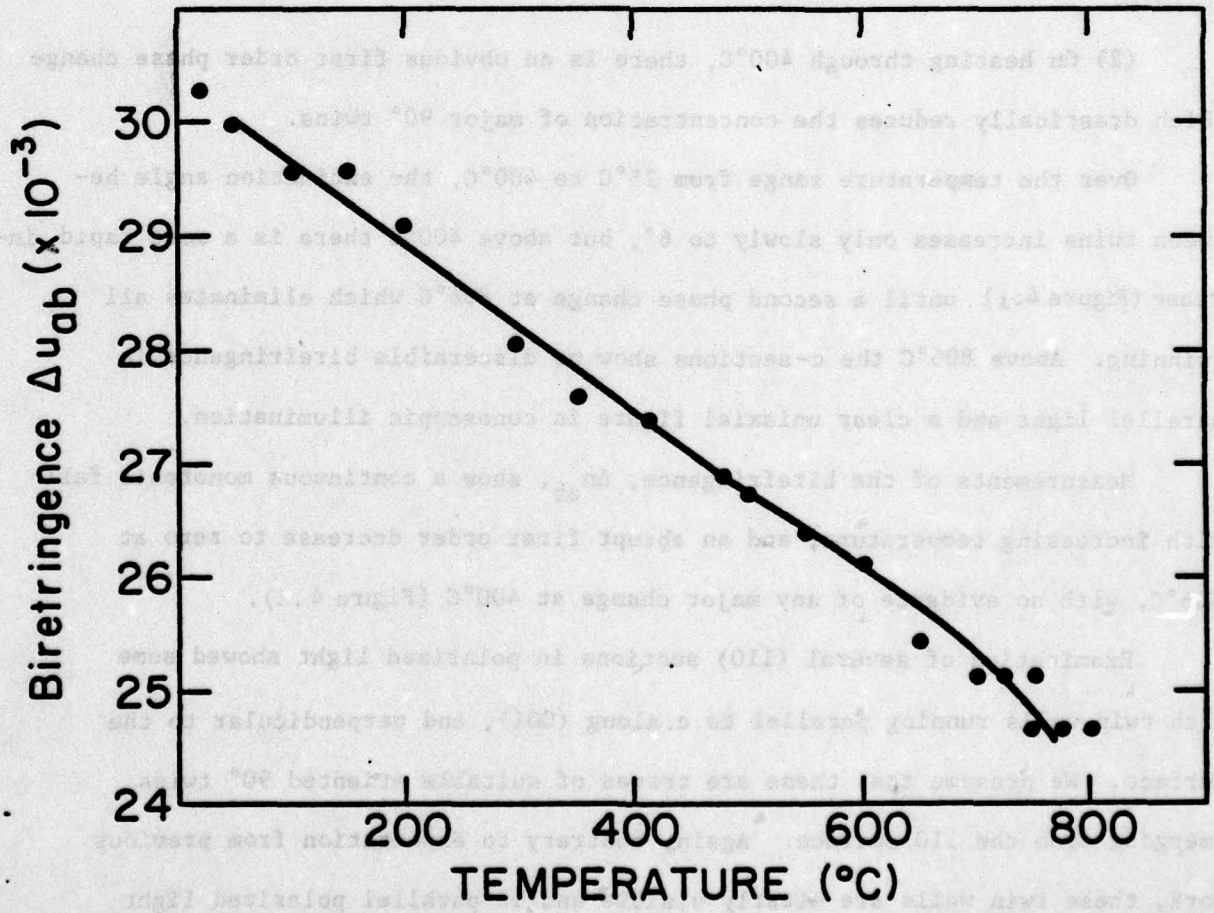

Fig. 4.2 Birefringence Δn_{ab} as a function of T in $Ba_2TiGe_2O_8$.

exhibit extinctions tilted by ∿3° away from the c direction (plate). This tilt of the indicatrix persists up to 400°C when there is an abrupt transition to straight extinction and the walls become invisible.

4.2.4 Preliminary X-Ray Studies

Preliminary x-ray studies, using Weissenberg photographs taken about the presumed tetragonal a-direction of the high-temperature cell, have given ambiguous results. The patterns contain odd, weak reflections in addition to the set of strong reflections, but if these weak reflections are ignored, the patterns can be indexed in terms of a pseudo-orthorhombic, possibly monoclinic unit cell with:

$$a_o = 8.60\text{Å}, \quad b_o = 8.66\text{Å}, \quad c_o = 5.35\text{Å}, \quad \gamma \simeq 90°$$

The pseudo-orthorhombic space group is Pba2. The weak reflections then possess non-integral indices in terms of this cell.

Kimura et al.[8] originally reported an orthorhombic cell in the space group Iba2, with:

$$a_o = 12.30\text{Å}, \quad b_o = 135.3\text{Å} \ (= 11a_o), \quad c_o = 10.70\text{Å}$$

No evidence for the long b-spacing could be found in the present data and Whatmore[10] has also cast doubt on its existence. If we assume a simplified form of Kimura's cell, with $b_o \simeq a_o$, Kimura's cell can be shown to reduce to the primitive pseudo-orthorhombic cell here reported by the transformation

$$\begin{vmatrix} 1/\sqrt{2} & 1/\sqrt{2} & 0 \\ 1/\sqrt{2} & -1/\sqrt{2} & 0 \\ 0 & 0 & 1/2 \end{vmatrix}$$

Work is proceeding to resolve the uncertainties in the unit cell and to account for the non-integral reflections.

4.2.5 Discussion

Optical data for our Czochralski-grown $Ba_2TiGe_2O_8$ crystals are clearly in contradiction to the present assigned symmetries in this crystal in that:

(1) For point group mm2, the principal axes of the indicatrix must coincide with the crystallographic axes, thus the tilt of extinction directions between 90° twins would be dictated by the a/b ratio, giving, from the data of Kimura et al.[8], 0.042°. To account for the major tilting observed, above 400°C the crystal must be in point group 2, where the indicatrix is free to rotate in the ab plane.

(2) Below 400°C, the tilting of the indicatrix away from the '$\underline{c}$' (001) axis suggests a further reduction in symmetry consistent with triclinic point group 1.

(3) Preliminary x-ray measurements give clear indication of a slight shear in (010), and the apparent complexity of the cell chosen by Kimura et al., together with its relationship to the primitive pseudo-cell, may also point towards a true triclinic unit cell.

Thus the preliminary indications are that in the Czochralski grown crystals which we are studying the transition sequence on heating is

$$1 \rightarrow 400°C \rightarrow 2 \rightarrow 806°C \rightarrow 4mm$$

i.e. the species would be

4mmF2	Ferroelastic not ferroelectric
4mmF1	Divertable but irreversible Ferroelectric;fully ferroelastic

5 Glass Ceramic Composites

Glasses in the lithium silicate family have been used to explore a completely new technique for generating polar polycrystal ceramics with oriented microstructure. In these studies, thin sheets of homogeneous glass with a composition close to $Li_2Si_2O_5$ were prepared and polished to 250 μ thickness. Using sputtered gold electrodes, the glasses were recrystallized under electric field. A number of different combinations of conditions were tried. Initial indications are that highly oriented columnar crystals of the meta and disilicates can be generated by performing the inital nucleation at low temperatures under high DC field, then growing the crystals to larger dimension under higher temperature at reduced or zero field.

For the oriented microcrystals the permittivity measured at 1 kHz $\varepsilon \simeq 6.0$, tan δ is exceedingly small, and the pyroelectric coefficient is of order 10^{-9} C/cm^2/°K.

References

1. K. Aizu, Phys. Rev. 146, 423 (1966).
2. L.A. Shuvalov, Suppl. J. Phys. Soc. Japan 28, 38 (1970).
3. H. Schmid, Solid State Comm. 5, 31 (1967).
4. H. Schmid, J. Phys. Chem. Solids 26, 973 (1965).
5. H. Schmid, Phys. Stat. Sol. 37, 209 (1970).
6. R. Masse A. Durit, Bull. Sco. Fr. Min. Cryst. 90, 407 (1967).
7. G. Blasse, J. Inorg. Nucl. Chem. 30, 2283 (1968).
8. M. Kimura, K. Doi. S. Nanamatsu, T. Kawamura, Appl. Phys. Lett. 23, 531 (1973).
9. M. Kimura, K. Utsumi, S. Nanamatsu, J. Appl. Phys. 47, 2249 (1976).
10. R. Whatmore, Private communication.

Appendix 1

Magnetoferroelectricity in Cr_2BeO_4

Magnetoferroelectricity in Cr_2BeO_4

R. E. Newnham, J. J. Kramer,[a] W. A. Schulze, and L. E. Cross

Materials Research Laboratory, Pennsylvania State University, University Park, Pennsylvania 16802
(Received 15 March 1978; accepted for publication 25 May 1978)

Chromium chrysoberyl undergoes a phase transformation from a paramagnetic state to a complex antiferromagnetic state at 28 K. The spiral spin structure of the antiferromagnetic state violates all the crystallographic symmetry elements, making Cr_2BeO_4 potentially ferroelectric. Chynoweth experiments conducted at low temperatures reveal a weak pyroelectric effect which disappears above 28 K. Cr_2BeO_4 ceramics can be poled electrically between 24 and 28 K, giving rise to remnant polarizations four to six orders of magnitude smaller than normal ferroelectrics. The pyroelectric coefficient and the remnant polarization reverse in sign with the poling field, but no anomalies in the electric permittivity or electric conductivity occur at the Nèel point.

PACS numbers: 77.80.−e, 75.80.+q, 77.70.+a, 75.50.Ee

Recent research on ferroelectrics has led to a growing interest in the fundamental causes of ferroelectric phase transitions, focusing especially on soft modes, order parameters, and improper transitions. There has also been an increasing awareness of cross-coupled domain phenomena caused by electric, elastic, and magnetic interactions. Lithium ammonium tartrate, for instance, is a type of *elastoferroelectric* in which mechanical strain is the primary order parameter at the 98 K phase transition. Strain gives rise to ferroelectricity through piezoelectric coupling with the polarization.[1] The opposite effect occurs in sodium potassium tartrate (rochelle salt) where electric polarization is the primary order parameter. Domains can be switched with mechanical stress as well as with electric fields because of the small spontaneous strain resulting from piezoelectric coupling to the polarization. Since the ferroelastic effect has its origin in an electric instability, we refer to its as *electroferroelasticity*.

Four other cross-coupled effects arise when magnetic phenomena are included. There are a number of examples of *elastoferromagnetism* and *magnetoferroelasticity* and at least one good example of *electroferromagnetism*: nickel iodine boracite.[2] At room temperature, NiI boracite is cubic, point group $\bar{4}3m$. Below room temperature at 120 K, it undergoes a transition to an antiferromagnetic state as the Ni^{2+} moments align; at this stage, the material is an antiferromagnetic piezoelectric, but it is neither ferromagnetic nor ferroelectric. On further cooling, a second phase transition to an orthorhombic ferroelectric state takes place at 64 K. As the crystal structure develops a spontaneous polarization, the magnetic structure is also altered, destroying the balance of spins in the antiferromagnetic state and producing a weak ferromagnetism. The ferromagnetic effect is of electric origin and can be referred to as an *electroferromagnet*. We have described this effect in some detail because it is the opposite of a *magnetoferroelectric*, the subject of this investigation.

A magnetoferroelectric develops a reversible spontaneous electric polarization on passing through a magnetic phase transition. The one-dimensional model in Fig. 1 illustrates the principle of a magnetically induced ferroelectric. At high temperatures, the system is paramagnetic and nonpolar with the paramagnetic cations located on centers of symmetry. On cooling through the Néel point, the system becomes antiferromagnetic with spins aligned along the chain direction. The spins order in such a way that each magnetic ion has one neighbor with parallel spin and one with antiparallel spin. The inversion centers are destroyed by magnetic order, making the chain a polar axis. Small atomic movements take place because of the differences in interatomic forces between atom pairs with parallel spin and atom pairs with antiparallel spin.

If the cations move in the same direction, as in Fig. 1, an electric polarization is produced. The atomic displacements destroy the centers of symmetry and make the material pyroelectric, piezoelectric, and potentially ferroelectric. The expected polarization is small because most magnetic transitions show second-order behavior with very small magnetostrictive effects.

No magnetoferroelectrics are known at present, although three possibilities have been suggested.[3] Bismuth manganate ($BiMn_2O_5$), calcium manganate ($CaMn_2O_4$), and terbium chromite ($TbCrO_3$) show the required symmetry change. We have searched the magnetics literature and found more than 30 other potential magnetoferroelectrics. The compilations by Oles and co-workers[4] and by Connolly and Copenhaver[5] were helpful in this regard. Most of the potential magnetoferroelectrics are antiferromagnetic with low transition temperatures and complex magnetic struc-

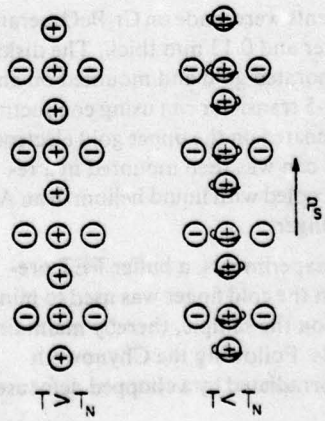

FIG. 1. Paramagnetic and antiferromagnetic states in a hypothetical magnetoferroelectric in which arrows indicate spin directions. Centers of symmetry are destroyed at the magnetic transition, converting the chain to a polar axis.

[a]On leave from the University of Delaware, Newark, Delaware 19702.

 0021-8979/78/4912-6088$01.10

tures, far more complicated than the model structure in Fig. 1. The material chosen for detailed investigation was chromium chrysoberyl, Cr_2BeO_4, one of the few good electrical insulators among the candidate compounds.

Cr_2BeO_4 is orthorhombic and isostructural with the minerals chrysoberyl (Al_2BeO_4) and forsterite (Mg_2SiO_4). The crystal structure consists of a close-packed lattice of oxygen ions with Cr^{3+} in octahedral sites and Be^{2+} in tetrahedral positions. At room temperature, Cr_2BeO_4 is paramagnetic and centrosymmetric and, therefore, nonpiezoelectric, nonpyroelectric, and nonferroelectric.

Low-temperature magnetic susceptibility measurements[6] show a cusp-shaped peak at 28 K characteristic of a paramagnetic-antiferromagnetic transition. The magnetic structure determined by neutron diffraction[7] at 4.5 K is a cycloidal spiral with a periodicity of about 65 Å, roughly 12 unit-cell lengths. Antiferromagnetic resonance experiments[8,9] confirmed the spiral structure and Néel temperature. The symmetry of the magnetic structure is triclinic, point group 1, making chromium chrysoberyl potentially magnetoferroelectric below 28 K.

Chromium chrysoberyl ceramics are prepared by calcining the coprecipitated metal-ion hydroxides. An intimate mixture was obtained by reacting mixed standard solutions of aluminum sulfate, chromium nitrate, and beryllium sulfate with ammonium hydroxide. The powder was dry pressed and then sintered at 1300 °C for 48 h to produce green-colored ceramics with resistivities greater than 10^7 Ω m. The crystal structure was confirmed by x-ray diffraction.

The properties of a magnetically induced ferroelectric are expected to differ radically from conventional ferroelectrics, since the atomic displacements are much smaller. Dielectric and piezoelectric coefficients are likely to be small, but domain walls should move easily, just as they do in most magnetic materials. In this case, however, domain-wall motion is controlled by electric fields rather than magnetic fields, and the resultant signal is electric charge rather than magnetic charge.

Five types of experiments were performed on polycrystalline Cr_2BeO_4: pyroelectric measurements, thermal depoling, pulse poling, complex permittivity measurements, and optical second-harmonic generation. The first three experiments gave evidence of ferroelectric behavior.

Electrical measurements were made on Cr_2BeO_4 ceramic disks 2.8 mm in diameter and 0.13 mm thick. The disks were electroded with evaporated gold and mounted on an alumina substrate in a TO-5 transistor can using conducting epoxy. Carbon black was coated on the upper gold electrode to absorb light. The TO-5 can was then mounted in a recessed copper holder and cooled with liquid helium in an Air Products LT-3-110 cold finger.

For the pyroelectric experiments, a buffer FET preamplifier positioned within the cold finger was used to minimize loading capacitance on the sample, thereby maintaining reasonable signal levels. Following the Chynoweth method,[10] the sample was irradiated by a chopped defocused

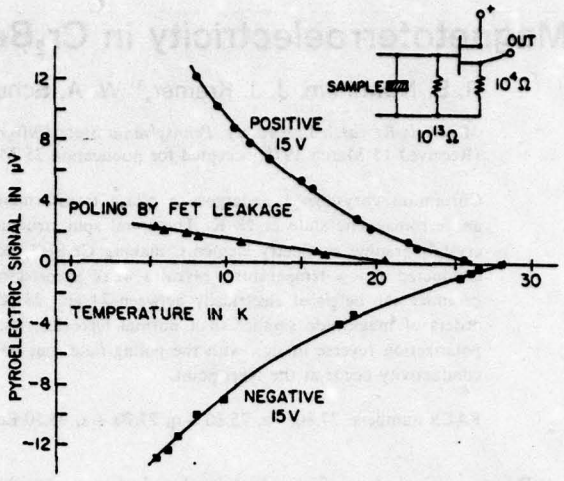

FIG. 2. Pyroelectric signal from Cr_2BeO_4 ceramics plotted as a function of temperatures.

1-mW He-Ne laser and the resulting pyroelectric signal detected with the aid of a lock-in amplifier.

For the initial pyroelectric measurements, the sample was poled with a field of 0.12 MV/m while cooling through the transition region. A signal was observed in the order of microvolts and was found to reverse in sign when poling was conducted with opposite polarity. If the supply voltage to the preamplifier was left on, a low level of poling was observed due to the leakage through the FET.

The level of pyroelectric signal as a function of temperature is illustrated in Fig. 2. Because of rapidly changing specific heat in this region, it is difficult to define the temperature change ΔT, but if a T^3 relation is assumed for specific heat, a more normal pyroelectric response is calculated.

Below about 24 K, the magnitude of the pyroelectric signal is reversible with temperature. When the temperature is raised above 24 K, however, the signal degrades and does not increase significantly with decreasing temperature. It appears that this is a transition region in which portions of the ceramic depole may only be repoled by an external bias.

Poling by any method other than cooling through the transition region under bias was only marginally successful. Small pyroelectric signals could be induced from a thermally depoled ceramic by poling with fields of 5 MV/m at 10 K. Attempts to reverse poling with up to 6 MV/m results in only very weak signals of opposite sign, showing that the coercive field increases rapidly below 24 K.

Calibration of the polarization levels observed in the pyroelectric experiments was achieved by thermal depoling. The absorbing surface of the sample was exposed to light from a 750-W projector lamp, and the resulting pyroelectric charge was collected with an integrating electrometer. When connected in a feedback mode, the system was capable of measuring charges less than 1 pC.

The polarization level is defined by the voltage applied as the sample was cooled through the transition region and by the discharge temperature. Once the polarization was in-

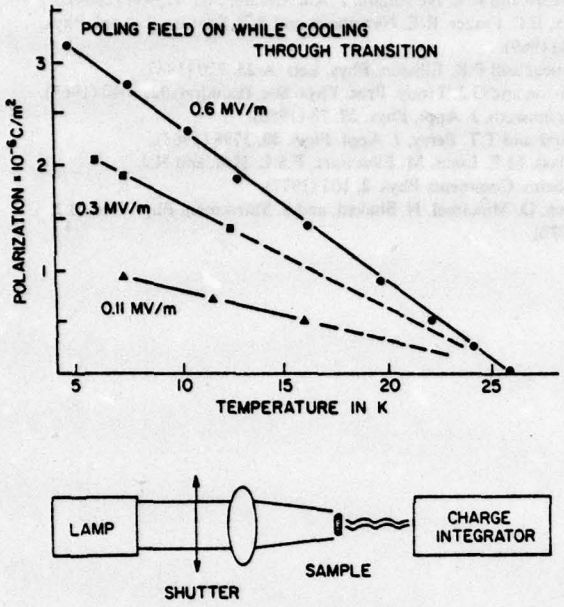

FIG. 3. Thermal depoling of Cr_2BeO_4 ceramics.

duced by the poling field, there appeared to be no degradation with temperature cycling below the transition region and with waiting periods up to 45 min. As shown in Fig. 3, Cr_2BeO_4 exhibits a linear dependence of polarization of the poling field and temperature. No saturation in polarization at low temperatures was observed in depoling experiments for poling fields ranging from 0.1 to 0.6 MV/m. Experiments at 7 K indicate a linear field dependence over 6 MV/m.

The temperature range in which maximum polarization is achieved for a given poling field lies between 24 and 28 K, in agreement with the pyroelectric experiments. Poling below 24 K led to only small polarizations.

Pulse poling was attempted utilizing differential integrators. A 10-ms voltage pulse was applied through an operational power supply to the sample and a linear capacitor of similar value. By observing the difference in these signals, small nonlinearities could be detected. Pulse poling lessens the effect of leakage current and sample heating that trouble a normal Sawyer-Tower measurement.

Pulse poling proved no more effective in reversing the polarization below the transition region than did the steady application of a field used in the pyroelectric experiment, even through much higher fields were applied. Field levels up to 8 MV/m were applied in 10-ms pulses, but polarizations of less than 1 μC/m^2 could be induced, and these were not achieved consistently.

The complex permittivity of Cr_2BeO_4 was measured as a function of temperature at several frequencies and under different bias fields, but nothing unusual was observed. Capacitance and tanδ were measured at 1, 10, 100 kHz, and 1 MHz using an automatic bridge. A three-terminal configuration connecting the cold-finger housing and the TO-5 can to the guard held the stray capacitance to about 0.3 pF. The resistivity increased on cooling from room temperature to liquid-helium temperature, but the capacitance remained at 4.0 ± 0.1 pF over the entire range. There were no anomalies at the Néel temperature of Cr_2BeO_4. Bias fields as large as 1.5 MV/m had no effect on the results. The measurements were repeated at high ac fields using a transformer ratio bridge operating at 100 Hz, 1 kHz, and 10 kHz. No change in ϵ or tanδ was observed in fields as large as 0.7 kV/m.

Chromium chrysoberyl and about 20 other potential magnetoferroelectrics were also tested for acentricity by optical second-harmonic generation, but with negative results. Our apparatus is similar in design to the SHG powder experiment described by Kurtz and Perry.[11] Second-harmonic signals as small as 0.001 times that of a comparable quartz specimen could be detected, but none were observed, either above or below the Néel points. The sensitivity of the experiment was hampered by absorption (all the specimens were colored) and by spurious light originating from a plasma in the evacuated low-temperature sample chamber. In any case, there was no evidence for acentricity from the SHG experiments.

In summary, when poled electrically, chromium chrysoberyl shows a pyroelectric effect in its antiferromagnetic state. The sign of the pyroelectric coefficients changes when the bias field is reversed. The reversible spontaneous polarization in the magnetoferroelectric state is approximately a million times smaller than that of $BaTiO_3$.

The influence of a magnetic phase transition on the spontaneous polarization of a pyroelectric has been described in a recent publication by Glass and co-workers.[12] Barium nickel fluoride ($BaNiF_4$) is a normal ferroelectric with a spontaneous polarization of 0.07 C/m^2, but at low temperatures, the nickel spins align antiferromagnetically causing a pronounced anomaly in the dynamic pyroelectric signal. The magnetic contribution to the spontaneous polarization is 0.9 mC/m^2, about two orders of magnitude smaller than P_s, and is proportional to the magnetic specific heat.

The reversible spontaneous polarization in Cr_2BeO_4 is approximately a thousand times smaller than the magnetic contribution to the spontaneous polarization of $BaNiF_4$ and about a hundred times smaller than the polarization predicted theoretically.[13] Goshen and co-workers also predicted[13] that the changes in electric susceptibility accompanying a magnetically induced ferroelectric transition would be too small to measure. This is consistent with the permittivity measurements on Cr_2BeO_4.

Magnetoferroelectrics are a type of improper ferroelectric, like gadolinium molybdate, in which polarization is not the order parameter driving the transformation. Because of the weakness in coupling between magnetic and electric effects, magnetoferroelectrics might be termed the ultimate impropriety.

ACKNOWLEDGMENTS

This work was sponsored by the Army Office of Research and Development (DAA 29-76-G-0145). We also wish to thank our colleagues at the Materials Research Laboratory for their advice and assistance.

[1]A Sawada, M. Udagawa, and T. Nakamura, Phys. Rev. Lett. 39, 829 (1977).
[2]H. Ascher, H. Rieder, H. Schmid, and H. Stössel, J. Appl. Phys. 37, 1404 (1966).
[3]S. Goshen, D. Mukamel, H. Shaked, and S. Shtrikman, J. Appl. Phys. 40, 1590 (1969).
[4]A. Oles, F. Kajzar, M. Kucab, and W. Sikora, *Magnetic Structures Determined by Neutron Diffraction* (Panstwowe Wydawnictwo Naukowe, Warsaw, 1976).
[5]T.F. Connolly and E.D. Copenhaver, *Solid State Physics Literature Guides* (Plenum, New York 1972), Vol. 5.
[6]R.P. Santoro and R.E. Newnham, J. Am. Ceram. Soc. 47, 491 (1964).
[7]D.E. Cox, B.C. Frazer, R.E. Newnham, and R.P. Santoro, J. Appl. Phys. 40, 1124 (1969).
[8]J.H. Ranicar and P.R. Elliston, Phys. Lett. A 25, 720 (1967).
[9]P.R. Elliston and G.J. Troup, Proc. Phys. Soc. (London) 92, 1040 (1967).
[10]A.G. Chynoweth, J. Appl. Phys. 27, 78 (1956).
[11]S.K. Kurtz and T.T. Perry, J. Appl. Phys. 39, 3798 (1968).
[12]A.M. Glass, M.E. Lines, M. Eibschutz, F.S.L. Hsu, and H.J. Guggenheim, Comments Phys. 2, 103 (1977).
[13]S. Goshen, D. Mukamel, H. Shaked, and S. Shtrikman, Phys. Rev. B 2, 4679 (1970).

Appendix 2

Crystal Growth of the Corundum-Type Iron and Chromium Oxide Solid Solution by Chemical Transport Reaction

CRYSTAL GROWTH OF THE CORUNDUM-TYPE IRON AND CHROMIUM OXIDE SOLID SOLUTION BY CHEMICAL TRANSPORT REACTION

K. Hayashi, A. S. Bhalla, R. E. Newnham and L. E. Cross

Materials Research Laboratory
The Pennsylvania State University
University Park, Pennsylvania 16802

Single crystals of corundum-type $(Fe,Cr)_2O_3$ solid solutions in the range 13.5 to 32.5 mole % Fe_2O_3 are of interest as potential magnetoferroelectric materials. Homogeneous single crystals in the form of hexagonal platelets of dimensions 2.0 x 1.0 x 0.5 mm were grown by a chemical vapor transport technique using Cl_2 as the transporting agent. Because of the thermal gradient used in the transport reaction, the composition of the crystals differs from that of the starting charge, but a simple thermodynamic analysis is given which permits the accurate prediction of the crystal composition for the range of growth parameters used in these studies.

INTRODUCTION

The solid solutions of iron and chromium oxides with the corundum structure are known to be antiferromagnetic with interesting spiral and cycloidal magnetic structures [1]. The low symmetry of these magnetic structures make the solid solution potentially magnetoferroelectric, an unusual type of ferroelectricity induced by magnetic spin alignment. Chromium chrysoberyl (Cr_2BeO_4), the first reported magnetoferroelectric [2], also has a cycloidal magnetic structure below its Neél temperature of 28 K [3]. For the solid solution series $(Fe_xCr_{1-x})_2O_3$ with $0.2 < x < 0.35$, the transitions to the helical magnetic state lie between about 150 K and 300 K, considerably higher than Cr_2BeO_4. This paper describes the growth of the required single crystals to examine the magnetoferroelectric effect in $(Fe_xCr_{1-x})_2O_3$ series.

There are a number of reports on single crystal growth of the oxides Fe_2O_3 and Cr_2O_3 [4-7]. Single crystals of Fe_2O_3 and Cr_2O_3 have been grown by vapor transport techniques using HCl [6] and chlorine [7] as the transport agents, and the flux method has been used to grow crystals of iron and chromium oxide solid solutions [8]. Chemical analysis of the solid solution crystal showed a maximum 1 mole % Fe_2O_3, even though 30 mole % Fe_2O_3 was introduced into the starting composition. Single crystals of the solid solution with composition higher than 1 mole % Fe_2O_3 have not been grown to date.

This paper describes the growth and characterization of single crystals of iron-chromium oxide solid solution single crystals in the 10 mole % to 40 mole % Fe_2O_3 range by a vapor transport method. A simple expression for the composition differences between the crystal and the starting solid solution mixture is derived in this study.

EXPERIMENTAL

Chlorine gas and hydrogen chloride are the most commonly used transport agents in oxides single crystal growth [9]. In the present investigation, $FeCl_3$ was used for the chlorine source because it is easy to handle. $FeCl_3$ produces Cl_2 gas on reacting with oxygen:

$$FeCl_3 + \frac{3}{4} O_2 \rightleftharpoons \frac{1}{2} Fe_2O_3 + \frac{3}{2} Cl_2 \uparrow. \quad (1)$$

The Gibbs free energy of this reaction shown in Fig. 1 was calculated from Barin's data [10]. It is clear from this free energy curve that Cl_2 gas would be produced as long as oxygen is supplied. Thus the expected chemical transport reactions could be represented as follows:

For the transport of chromium oxide

$$2CrCl_3 + \frac{3}{2} O_2 \rightleftharpoons Cr_2O_3 + 3Cl_2 \quad (2)$$

and for the transport of iron oxide

$$2FeCl_3 + \frac{3}{2} O_2 \rightleftharpoons Fe_2O_3 + 3Cl_2. \quad (3)$$

The sublimation points of ferric chloride and chromium chloride are 592 K and 1218 K respectively. In the present experiment, where the reaction takes place above 1040 K, ferric chloride is completely in the gaseous phase. The vapor pressure of chromium chloride over this temperature range is more than 30 mmHg [10], and thus chromium chloride is also partly gaseous above 1040 K.

The changes in free energy for reactions (2) and (3) are plotted as a function of temperature in Fig. 1. At low temperature, the right-hand components of the equilibrium equations are more stable than at high temperature, favoring the production of oxides at low temperatures. Therefore the low

temperature region is the crystallization zone, whereas high temperatures favor vaporization.

CRYSTAL GROWTH

Preparation of the Starting Materials and Growth Runs

The chemical transport reaction includes a gas-solid reaction. The reaction rate depends on the surface area of the solid material, so that powders of small particle size are desirable as starting materials. To prepare a fine powder of the solid solution, the nitrate decomposition reaction was used. Ferric nitrate $Fe(NO_3)_3 \cdot 9H_2O$ (Baker Chemical Co. with impurities of SO_4^{-2}: <0.01%, Mn^{+2}: 0.005%, Cl^{-1}: <5%) and chromium nitrate (Fisher Scientific Co. with impurities of Cl^{-1}: 0.001%, Fe^{+3}: 0.002%, SO_4^{-2}: 0.003%) were mixed in the proper ratios and placed in a ceramic crucible. It was then decomposed at 250°C for several hours. To complete the solid reaction, it was heated at 800°C for one day. The resultant solid solution powder had a particle size smaller than 1 μm as determined by scanning electron microscopy.

Weighed quantities of the Fe-Cr oxide solid solution powder (about one gram) were placed in quartz tubes of various dimensions (14 mmϕ, 10 cm long; 12 mmϕ, 10 cm long, and 8 mmϕ, 10 cm long). Anhydrous ferric chloride (about 50 mg) was then added to the oxide powder. The quartz tube was evacuated and then backfilled with pure oxygen (10^{-2} atm) and sealed.

The sealed ampule was placed in a temperature gradient furnace (Fig. 2) with the end containing the solid solution powder in the high temperature zone (1040 C run A, 1070 C run B). The positions of the crystals and the residuals are shown in Fig. 2. In some exepriments the residuals were separated into two well defined areas.

Results and Characterization of Single Crystals

After one day to one week reaction, the quartz ampule was quenched to room temperature in air. The experimental conditions and the results are presented in Table I. Chemical compositions were determined by x-ray fluorescence spectroscopy, yielding an iron to chromium ratio accurate to within 1%. The crystals and residual powder were washed with water and alcohol several times, then dried and weighed.

The chemical compositions of the crystals and the residual materials differed from that of the starting material. The iron content of the crystals was always higher than that of the starting solid solution, and the residue was correspondingly depleted in iron.

The crystals were generally hexagonal platelets (Fig. 3) with the trigonal c-axis perpendicular to the major surface. Typical dimensions of the single crystals were about 2.0 x 1.0 x 0.5 mm^3. The single-crystal nature of the specimens, together with the crystallographic orientations were determined by x-ray diffraction using a Weissenberg camera.

The composition distribution in a number of single crystals was determined by x-ray emission analysis in a SEM, by scanning across the surface of the crystal. The results indicated that the chemical composition in all the crystals was homogeneous. Figure 4 shows the scan for a crystal containing 32.5 mole % iron oxide. The traces revealed no evidence of chlorine.

DISCUSSION

In the present study, the detailed mechanisms of the chemical transport were not of primary interest. The effort was directed towards the growth of crystals for a specific experimental requirement, and the primary need was for

a simple method of predicting and controlling the composition of the crystals and relating this to the composition of the starting charge and to the growth conditions.

Since preliminary experiments showed that the concentration difference between residue and crystals was not a function of $FeCl_3$ concentration nor of the transport rate, and that the cross-section area of the ampule did not greatly affect the transport rate (Fig. 5), it was assumed as a first approximation that growth might be occurring in quasi-equilibrium conditions. Under these circumstances with $(Fe_yCr_{1-y})_2O_3$ representing the composition of the crystal and $(Fe_zCr_{1-z})_2O_3$ the composition of the residue, if we neglect gas diffusion and Knudsen effects which are very small, then the partial pressures are constant throughout the ampule, and the system can be considered in two parts:

1. $(Fe_yCr_{1-y})_2O_3$ in equilibrium with the gases of P_{O_2}, P_{Cl_2}, P_{FeCl_3}, and P_{CrCl_3} at the temperature of the growth end T_1.
2. $(Fe_zCr_{1-z})_2O_3$ again in equilibrium with the gases P_{O_2}, P_{Cl_2}, P_{FeCl_3}, P_{CrCl_3} but now at the temperature of the charge end of the ampule T_2.

These equilibrium conditions can be described by the reactions

$$2(1-y)CrCl_3 + 2yFeCl_3 + \frac{3}{2}O_2 \rightleftharpoons (Fe_yCr_{1-y})_2O_3 + 3Cl_2 \qquad (4)$$

$$2(1-z)CrCl_3 + 2zFeCl_3 + \frac{3}{2}O_2 \rightleftharpoons (Fe_zCr_{1-z})_2O_3 + 3Cl_2 \qquad (5)$$

where the equilibrium constants for these reactions

$$K_p(T_1,y) = \frac{P_{Cl_2}^{\ 3}}{P_{CrCl_3}^{\ 2(1-y)}\ P_{FeCl_3}^{\ 2y}\ P_{O_2}^{\ 3/2}} \qquad (6)$$

$$K_p(T_2,z) = \frac{P_{Cl_2}^{3}}{P_{CrCl_3}^{2(1-z)} \; P_{FeCl_3}^{2z} \; P_{O_2}^{3/2}} \qquad (7)$$

These equilibrium constants may also be expressed in terms of the Gibbs free energy.

$$K_p(T_1,y) = \exp\,[-\Delta G(y)/RT_1] \qquad (8)$$

$$K_p(T_2,z) = \exp\,[-\Delta G(z)/RT_2]. \qquad (9)$$

Since y and z are reasonably close in this system, the simplifying assumption is made that $\Delta G(Y) \simeq \Delta G(z)$ and from equations (8) and (9)

$$[K_p(T_1,y)]^{T_1} = [K_p(T_2,z)]^{T_2}. \qquad (10)$$

On dividing equation (6) by (7) and making use of relation (10),

$$\left[\frac{P_{CrCl_3}}{P_{FeCl_3}}\right]^{2(T_1y-T_2z)} \times \left[\frac{P_{Cl_2}^{3}}{P_{CrCl_3}^{2} \; P_{O_2}^{3/2}}\right]^{(T_1-T_2)} = 1 \qquad (11)$$

which can be expressed as

$$y = \frac{T_2}{T_1}\,z + \left(\frac{T_2}{T_1} - 1\right)\alpha$$

where

$$\alpha = \ln\left[\frac{P_{Cl_2}^{3}}{P_{CrCl_3}^{2} \; P_{O}^{3/2}}\right] \Big/ \ln\left[\frac{P_{CrCl_3}}{P_{FeCl_3}}\right]^{2}. \qquad (12)$$

In Fig. 6 the concentration C_c in the crystal is plotted vs. the concentration C_R in the residue, which is in effect a plot of y vs. z. The open

circles were taken with (A) T_1 = 1113 K, T_2 = 1313 K and the closed circles with (B) T_1 = 1043 K and T_2 = 1343 K. If equation (12) is applied under these two sets of conditions,

$$y = 1.18\ z + 0.18\ \alpha \text{ (case A)} \tag{13}$$

$$y = 1.29\ z + 0.29\ \alpha' \text{ (case B)}. \tag{14}$$

The slope obtained experimentally is between 1.18 and 1.30, in remarkable agreement with the prediction of equation (12). Thus it would appear that in this system since C_c and C_R are not vastly different, the approximation $\Delta G(y) = \Delta G(z)$ is probably valid and crystal growth is taking place under close to equilibrium conditions. A number of the growth runs are summarized in Table I.

CONCLUSION

Single crystals of the solid solution $(Fe_xCr_{1-x})_2O_3$ with $0.1 < x < 0.4$ were grown by chemical vapor transport using $FeCl_3$ as the source of the transporting Cl_2 gas. The iron content of the crystals is always larger than that of residual solid solution source material. Based on the assumption that growth takes place under near equilibrium conditions and that the compositions are sufficiently close that the Gibbs free energies do not differ markedly, a simple relation has been derived which permits the prediction of the composition and temperature conditions required for a given crystal composition.

TABLE I

Growth conditions and the iron content of the starting charge, crystals and the residue.

Growth run	Starting material wt(mg)	Mole% of Fe_2O_3				Time of growth run (hours)	Transport rate (mg/hr)	$FeCl_3$ wt(mg)	Cross-section of the quartz tube (cm^2)*	Temperature gradient**
		Starting charge	Crystal	Residue I	Residue II					
1.25	1020	11.0	13.5	10.8	--	48	1.5	58	1.00	B
2.1	1316	11.0	15.0	9.0	10.5	48	4.1	48	1.00	A
3.2	805	13.0	17.2	12.5	--	96	4.4	54	0.50	A
2.13	997	16.7	19.3	15.0	--	30	5.3	45	1.00	A
2.4	1153	17.3	22.8	16.4	16.4	69	2.7	47	1.00	A
2.4(3)	1103	18.3	24.0	16.0	--	89	9.0	120	1.50	B
2.4(5)	1126	27.0	32.5	25.0	--	135	3.0	97	1.50	B

* Length of the tube in all the growth runs = 10 cm

**Temperature of the vaporization and crystallization zones

(A) T_2 = 1313 K T_1 = 1113 K

(B) T_2 = 1343 K T_1 = 1043 K

REFERENCES

[1] D. E. Cox, W. J. Kakei and G. Shirane. J. Phys. Chem. Solids 23, 405 (1963).

[2] R. E. Newnham, J. J. Kramer, W. A. Schulze and L. E. Cross. J. Appl. Phys. 49, 6088 (1970).

[3] D. E. Cox, B. C. Fraser and R. E. Newnham. J. Appl. Phys. 40 (3), 1124 (1969).

[4] A. A. Popova. Rost Kristallov. 4, 148 (1964).

[5] I. Sunagawa. Amer. Mineral. 45, 556 (1960).

[6] P. Kleiner. Z. anorg. allg. chem. 378, 71 (1970).

[7] P. Peshev, G. Bliznakov, G. Gyurov and M. Ivanova. Mat. Res. Bull. 8, 1011 (1973).

[8] R. E. Barks. PhD Thesis, The Pennsylvania State University (1966).

[9] H. Schäfer. Chemische Transportreaktion, verlag chemie, Weinheim (1962).

[10] I. Barin and O. Knacke. Thermochemical Properties of Inorganic Substances, Springer-verlag, New York (1973 and 1976 supplements).

FIGURE CAPTIONS

Fig. 1 ΔG vs. temperature for the chemical transport reaction. The free energy of gaseous $CrCl_3$ is obtained by extrapolation of the room temperature and 1218 K values.

Fig. 2 Temperature profile of the furnace and the position of the crystallization and the vaporization zones.

Fig. 3 (a) SEM photograph of intergrown crystals containing 32.5 mole % of Fe_2O_3 (x 50).

(b) Morphology of an individual crystal, SEM photograph (x 200).

Fig. 4 X-ray chemical analysis of a single crystal with the scanning direction parallel to the C-face.

Fig. 5 (a) Plot of (C_c-C_R) vs. amount of $FeCl_3$.

(b) Plot of (C_c-C_R) vs. transport rate.

(c) Plot of transport rate vs. cross-section of the quartz tube.

Open circles: temperature distribution (A).

Solid circles: temperature distribution (B).

Fig. 6 Relation between the mole % Fe_2O_3 in the crystals and that in the residual solid solution.

Open circles: temperature distribution (A).

Solid circles: temperature distribution (B).

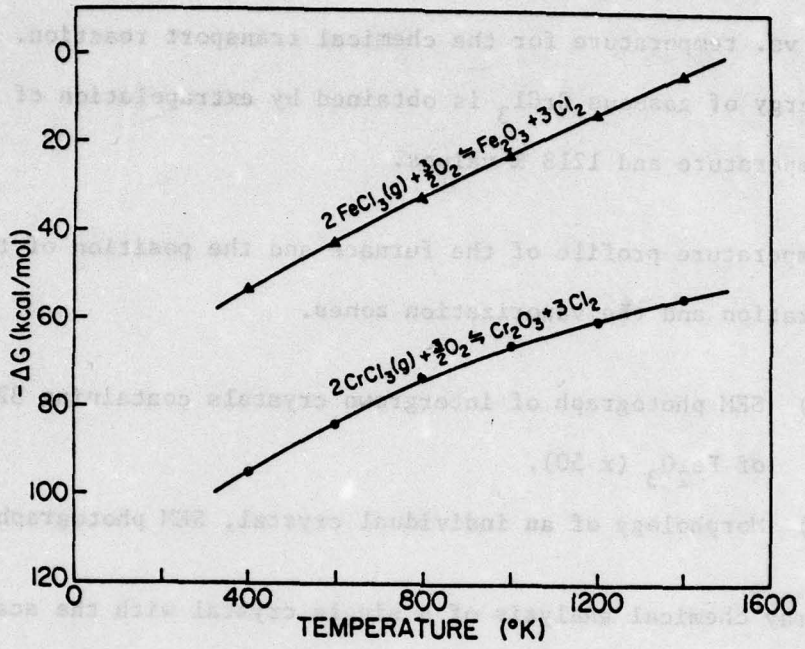

Figure 1

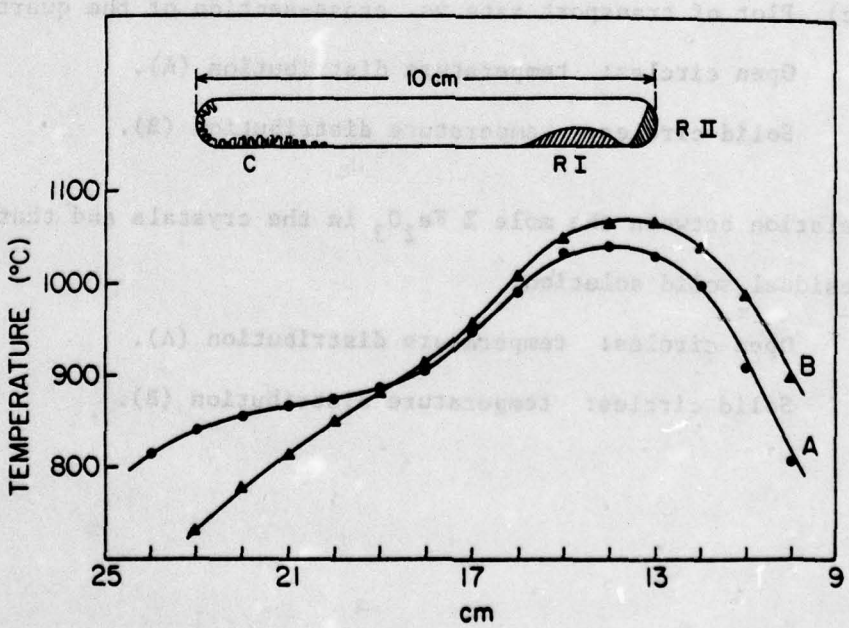

Figure 2

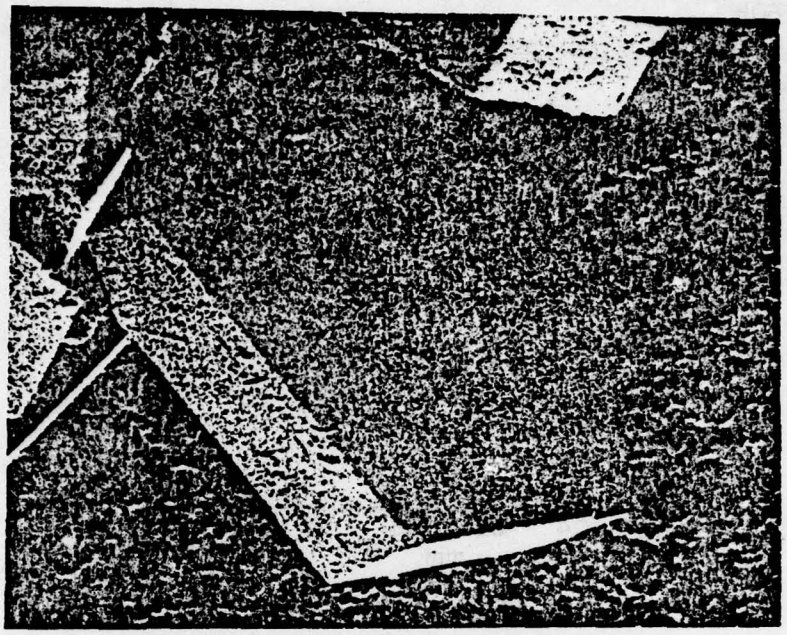

Figure 3

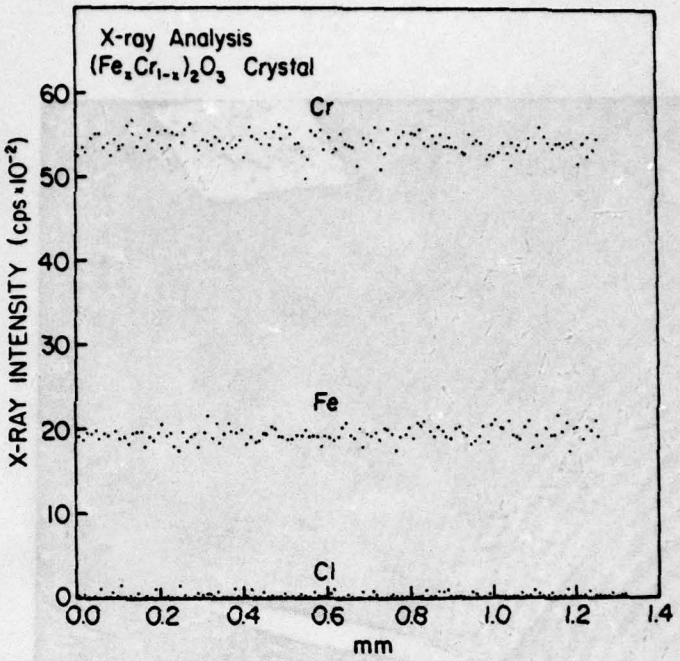

Figure 4

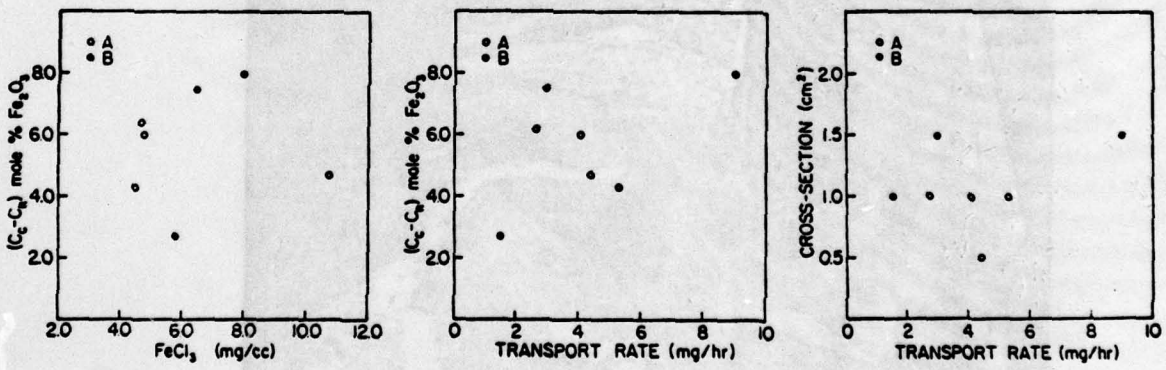

Figure 5

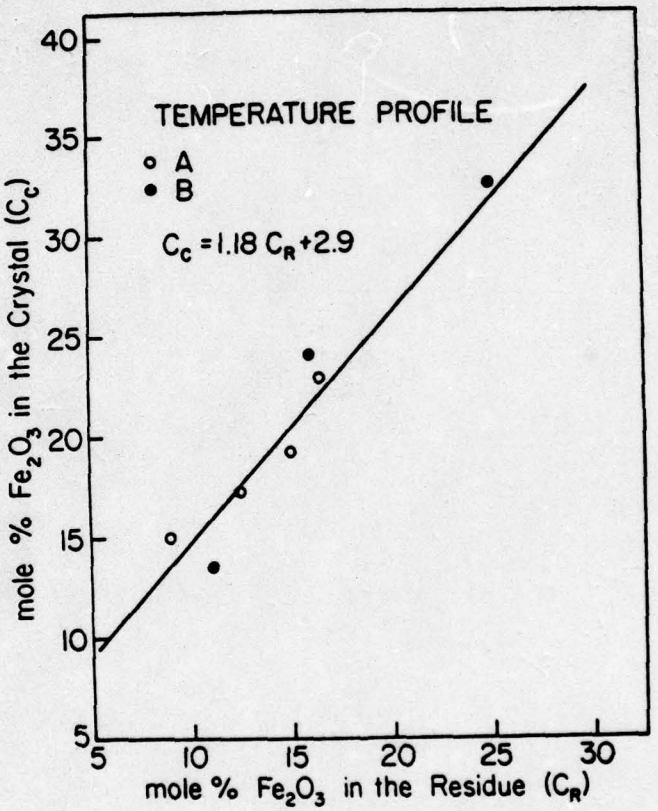
TEMPERATURE PROFILE
A
B
$C_c = 1.18\ C_R + 2.9$
mole % Fe_2O_3 in the Crystal (C_c)
mole % Fe_2O_3 in the Residue (C_R)
40
35
30
25
20
15
10
5
5
10
15
20
25
30

Figure 6

Appendix 3

Crystal Growth, Characterization and Electrical Properties of Corundum Type $(Cr_{1-x}Fe_x)_2O_3$ Solid Solution

CRYSTAL GROWTH, CHARACTERIZATION AND ELECTRICAL PROPERTIES OF CORUNDUM TYPE $(Cr_{1-x}Fe_x)_2O_3$ SOLID SOLUTION

by

K. Hayashi, A. S. Bhalla, L. E. Cross and R. E. Newnham
Materials Research Laboratory
Penn State University
University Park, PA 16802

The solid solution $(Cr_{1-x}Fe_x)_2O_3$ with $0{\cdot}2 < x < 0{\cdot}35$ are antiferromagnetic with interesting spiral and cycloidal magnetic structures. In view of its crystal structure this material is also expected to show magnetoferroelectric properties which are a most interesting form of improper ferroelectricity.

This paper reports the growth of $(Cr_{1-x}Fe_x)_2O_3$ by chemical vapor transport techniques using Cl_2 as a transport agent. Single crystals of dimensions $2{\cdot}5 \times 1{\cdot}0 \times 0{\cdot}5$ mm^3 were grown and characterized. The chemical composition of these crystals was found to be different than that of the starting chemical charge. A thermodynamical analysis is given to explain this compositional change which occurs during growth.

Some interesting electrical properties of these crystals were also measured and are discussed in this paper.

EXPERIMENTAL

Single crystals of $(Cr_{1-x}Fe_x)_2O_3$ were grown by chemical vapor transport techniques using Cl_2 as a transport agent(1). The expected transport reactions are as follows,

$2FeCl_3+3/2O_2 \rightleftarrows Fe_2O_3+3Cl_2$

$2CrCl_3+3/2O_2 \rightleftarrows Cr_2O_3+3Cl_2$

According to thermochemical calculations, the right hand side compounds of those equilibrium equations are more stabilized at low temperature. Therefore oxides are grown at the low temperature zones of the reaction tubes. Temperatures of crystallization zone and vaporization zone are around 800°C and 1050°C respectively. Single crystals of dimensions 2.5x1.0x0.5 mm^3 were grown. By chemical transport techniques, the iron content of crystals was always higher than that of the starting solid solution. Increment of iron content was proportional to iron content of the starting solid solution. The proportional constant was related to ratio of temperatures between vaporization and crystallization zones. But in a single crystal, iron and chromium concentrations are homogeneous . Crystals have hexagonal platelet shapes. The plate face is c-face of hexagonal lattice. The details were reported in a previous paper(1).

Using those single crystals, electrical resistances of c-direction were measured by dc two electrodes method. Gold was sputtered on c-faces of a single crystal as electrodes. Area of the electrodes was about 1 mm^2 and the thickness was about 0.05 mm. The crystals of 24.0%Fe_2O_3, 32.5%Fe_2O_3 and 38.2%Fe_2O_3 were used and resistances were measured from 90K up to 380K. The resistances against reciprocal temperatures are shown in Fig.1. The resistances of 24.0%Fe_2O_3 and 32.5%Fe_2O_3 crystals show abnormal changes around 170 and 330K respectively. Those temperatures correspond to magnetic transition temperatures(2-3). When the resistances are plotted against $1/T^{1/4}$ (Fig.2), linear changes of resistances are shown below Neél temperature. The lines indicate Mott's law is valid in those regions. In α-Fe_2O_3, HOPPING conductivity caused by non-localized Fe^{2+} impurity was suggested(4). In Cr_2O_3, activation energy of electrical coductivity changes at Neél temperature(5). The present experimnt proposes evidence of HOPPING conductivity and also suggests magnetic transition dependence-electrical conductivity.

According to Arnaudov(6), 4-types of HOPPING mechanism were defined. In $(Cr_{1-x}Fe_x)_2O_3$, Mott law dominated below Neél temperature. In Mott law, electrical resistivity is representd as

$$\ln\sigma = A - B/T^{1/4}.$$

In 32.5 and 38.2%Fe_2O_3 solid solutions, B-values are 8.10 and 7.70 respectively.

CONCLUSION

Single crystals of solid solution $(Cr_{1-x}Fe_x)_2O_3$ were grown by chemical vapor transport techniques using Cl_2 of transport agent. Iron content of the crystal is always higher than that of the starting solid solution. Difference of iron content between starting solid solution and crystal is proportional to iron content of the starting solid solution.

Electrical resistivity shows Mott law below Neel temperature. The on set temperature seams to depend on the Neél temperature.

REFERENCES

(1) K.Hayashi, A.S.Bhalla, L.E.Cross and R.E.Newnham, J.Cryst.Growth,(submitted)

(2) D.E.Cox, W.J.Takei and G.Shirane, J.Phys.Chem.Solids,23,405(1963)

(3) A.Knappworst, H.Lechert and W.Gunsser, Z.Phys.Chem.,47,207(1965)

(4) L.P.Fefilatiev, G.Demazeau, P.BPFabritchnyi and A.M.Babechkin, Solid State Commun.,28,509 (1978)

(5) W.C.Hagel, J.Appl.Phys.,36,2586(1965)

(6) B.G.Arnaudov, D.S.Domanevskii and I.Y.Yanchev, Phys.Stat.sol.,(b) 91,311(1979)

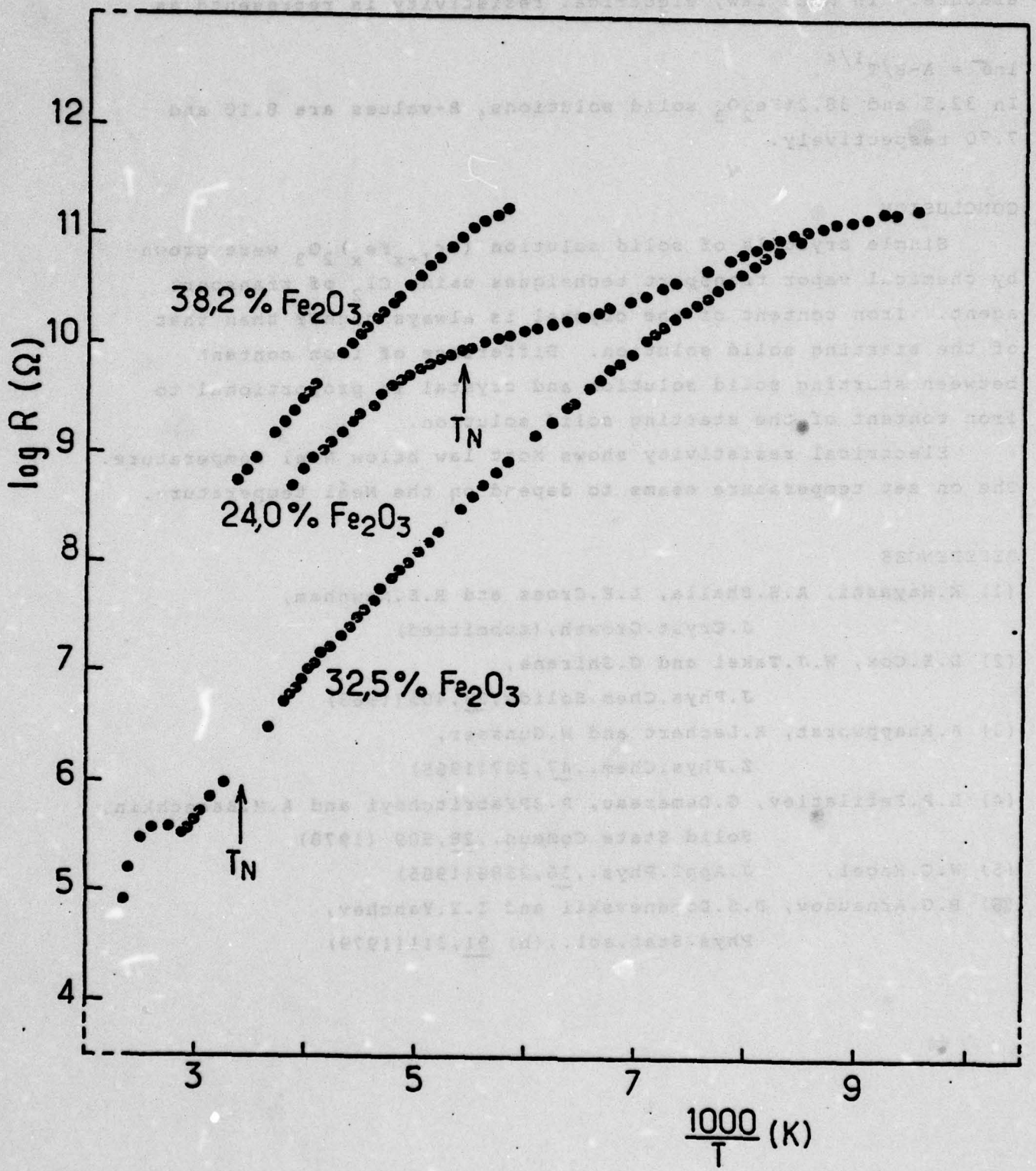
12
11
10
9
8
7
6
5
4
log R (Ω)
38,2 % Fe2O3
24,0 % Fe2O3
32,5 % Fe2O3
TN
TN
3
5
7
9
1000/T (K)

Figure 1

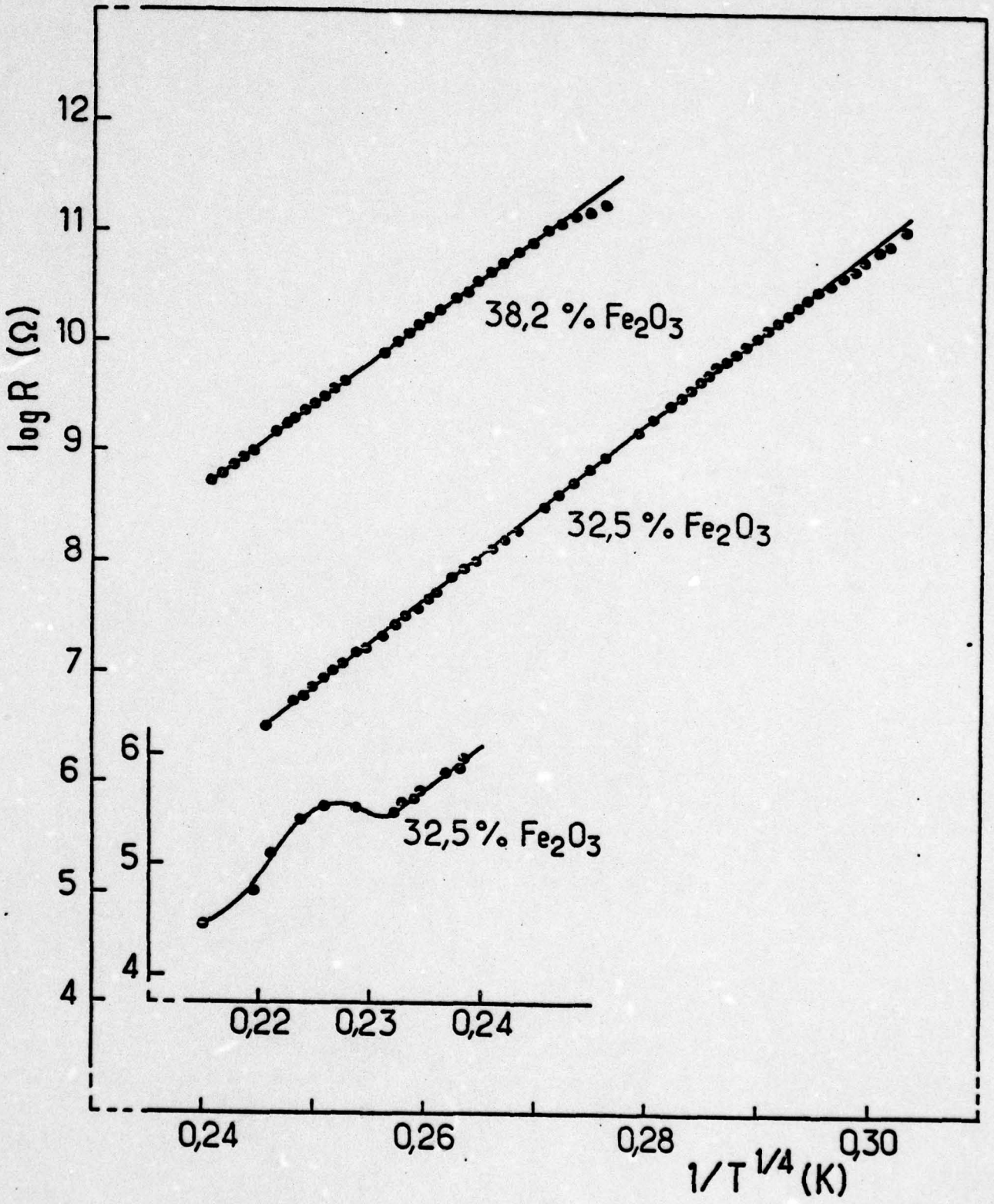
log R (Ω)
12
11
10
9
8
7
6
5
4
38,2 % Fe2O3
32,5 % Fe2O3
6
5
4
32,5 % Fe2O3
0,22
0,23
0,24
0,24
0,26
0,28
0,30
1/T 1/4 (K)

Figure 2

Appendix 4

Optical Second Harmonic Signals from Clay Minerals

Phys. Chem. Minerals 1, 379–384 (1977)

PHYSICS AND CHEMISTRY OF MINERALS

Optical Second Harmonic Signals from Clay Minerals

R.E. Newnham, J.J. Kramer*, W.A. Schulze, and G.W. Brindley

Materials Research Laboratory, The Pennsylvania State University, University Park, Pennsylvania 16801, U.S.A.

Abstract. Using a neodymium glass laser and time-synchronized pulse detection, second harmonic signals were observed from a number of clay mineral powders. The second harmonic generation (SHG) experiments provide the first physical evidence (other than diffraction patterns) for the polar nature of the kaolinite layer and its stacking sequences. Well-crystallized nacrite and dickite specimens gave signals comparable to those of quartz, but the SHG intensities from the smaller kaolinite and halloysite crystallites were noticeably weaker. Based on results from eight specimens, there appears to be a direct correlation between SHG intensity and particle size, similar to that reported previously for quartz.

Introduction

The discovery of lasers in 1960 was followed a year later by the discovery that optical harmonics could be generated when a noncentrosymmetric crystal was exposed to an intense laser beam (Franken et al., 1961). When irradiated with the red light of a ruby laser, quartz crystals emit blue light having twice the frequency of red light. Such an effect is called Second Harmonic Generation, or SHG for short. The SHG coefficients constitute a third-rank tensor similar in form to that of the piezoelectric coefficients.

Optical second harmonic generation is known to be a highly reliable and sensitive physical test for the existence of crystalline acentricity (Kurtz and Dougherty, in press). Although some of the initial experiments were done on natural quartz, the SHG test has not been exploited widely as a characterization method for minerals. In this paper, we report the observation of SHG signals from kaolinite and other fine-grained aluminosilicates. The kaolinite group includes three well-crystallized polymorphs (kaolinite, dickite, nacrite) and the partly disordered mineral halloysite. The basic structural unit is the kaolin

* On leave from the University of Delaware, Newark, Delaware 19711, U.S.A.

layer which consists of a pseudohexagonal sheet of silica tetrahedra superposed on a sheet of alumina octahedra. Kaolinite and its polytypes are noncentrosymmetric crystallizing in either triclinic point group 1 or monoclinic point group m, but the usual physical properties associated with acentricity (piezoelectricity, pyroelectricity, optical activity) have never been observed because of the small crystallite sizes. Second harmonic generation is a far more sensitive test, however, and provides direct physical evidence of acentricity in fine-grained materials.

During the past few years we have used second harmonic analysis as a routine screening test in searching for new piezoelectric transducer materials. The SHG experiment is a simple test which can be made in a few minutes and does not require expensive equipment[1]. Powder samples are prepared and packed into a sample holder similar in size to that of an X-ray diffractometer. To study phase transitions, sample temperatures can be controlled from liquid helium temperatures to 500° C, and polarizing optics make it possible to determine the orientation of polar axes in single crystals.

The apparatus illustrated in Figure 1 is sensitive to a wide range of SHG signals, extending about three orders of magnitude above and below the intensity of the signal from polycrystalline quartz. A neodymium glass laser provides coherent radiation at 1.06 μm in bursts of 10^{-3} s made up of 50–100 individual pulses. A photodiode and filter are placed in the entrance beam to monitor the incident pulses, and block unwanted background radiation.

The second harmonic radiation emanating from the sample is collected by a parabolic mirror and focused on a detector behind the sample. Cooling the photomultiplier tube of the detector to −40° C eliminates noise from thermionic emission. Filters placed in front of the detector photomultiplier transmit wavelengths within 200 A of the second harmonic and block the fundamental. The spectral purity of the SHG signal can be tested with narrow and broad band filters centered at the second harmonic frequency. Spurious signals with a broad band response show an increased intensity when the broad band filter is substituted for the narrow band filter, whereas the true second harmonic does not. To provide still greater sensitivity, photomultiplier pulses from the second harmonic can be synchronized to the fundamental pulses recorded by the photodiode in the entrance beam. Both the laser pulses and the resulting SHG signals are displayed on a dual-trace storage oscilloscope triggered by the incident laser pulse. The correlation between laser pulse and second harmonic signal eliminates spurious out-of-phase signals at the second harmonic wavelength from consideration. The detection system is more sensitive than the usual arrangement in which only the envelope of the laser burst is recorded.

Figure 2 shows SHG patterns obtained for powder specimens of nacrite, kaolinite, and pyrophyllite. The samples were packed in a glass sample holder using a few drops of collodion as a binder. Nacrite gives a second harmonic signal comparable to fine-grained quartz, but kaolinite gives much weaker signals, and the pyrophyllite specimen shows none at all, as would be expected for a centrosymmetric mineral. Eight specimens were tested in all. Dickite and

[1] Second harmonic equipment is available commercially from North American Philips, 345 Scarborough Road, Briarcliff Manor, N.Y., 10510, U.S.A.

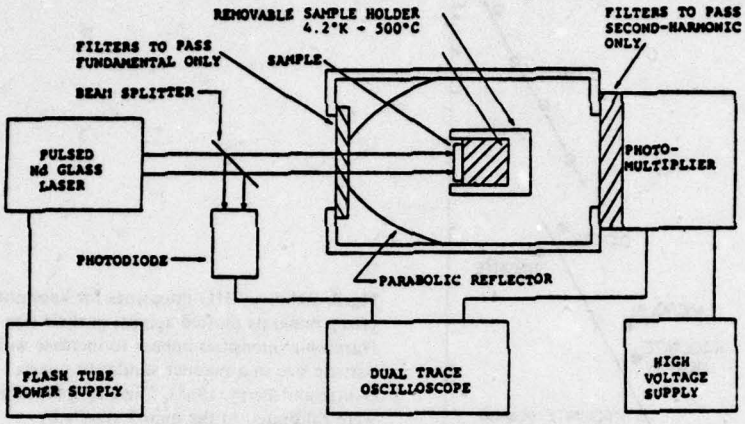

Fig. 1. A schematic of the apparatus used to observe optical second harmonic signals from clay minerals. The design is similar to that developed by Kurtz and Perry (1968)

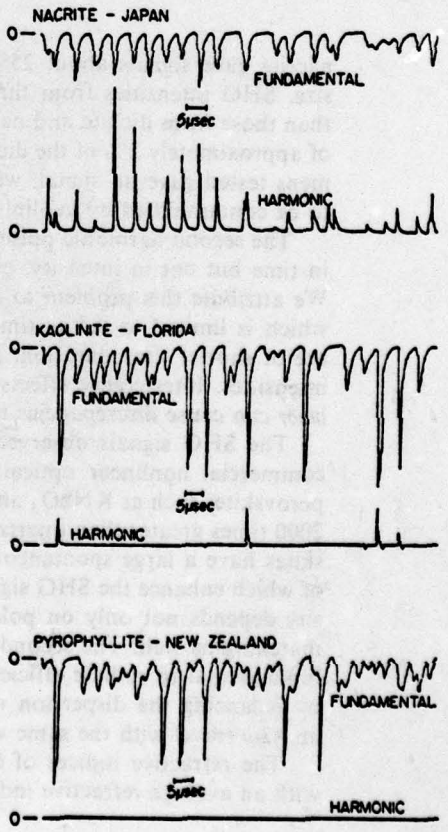

Fig. 2. Optical second harmonic tests on nacrite, kaolinite, and pyrophyllite. The dual trace oscilloscope patterns show the laser fundamental and the corresponding SHG pulses plotted as a function of time. The SHG signals from nacrite are comparable in intensity to those from quartz, but kaolinite gives much weaker signals and pyrophyllite gives none at all

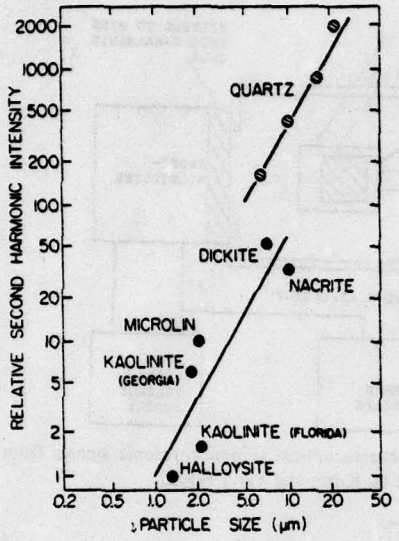

Fig. 3. Relative SHG intensities for kaolinite group minerals plotted against particle size. Harmonic intensities appear to increase with particle size in a manner similar to quartz (Kurtz and Perry, 1968). The clay intensities were calibrated to the quartz results by measuring the second harmonic from a novaculite specimen

nacrite gave signals about 25% of the intensity of quartz with similar grain size. SHG intensities from three kaolinite specimens were 5–10 times weaker than those from dickite and nacrite. Halloysite gave an exceedingly weak signal of approximately 2% of the dickite intensity. One of the two pyrophyllite specimens tested gave no signal, while the other gave a weak signal but was found to be contaminated by kaolinite.

The second harmonic pulses in Figure 2 correlate well with the fundamental in time but not in intensity, especially for the weak intensities from kaolinite. We attribute this problem to the sampling rate of the digital detection system which is limited to 0.5 μs time intervals. Many of the individual laser pulses are of shorter time duration. Mode interference is another factor affecting the intensities. Interference effects over the beam cross-section from a multimode laser can cause discrepancies of this type.

The SHG signals observed from the clay minerals are weak compared to commercial nonlinear optical materials used in device applications. Acentric perovskites such as $KNbO_3$ and $PbTiO_3$ give second harmonic intensities about 2000 times greater than quartz and about a million times halloysite. The perovskites have a large spontaneous polarization and large refractive indices, both of which enhance the SHG signal (Kurtz and Perry, 1968). But harmonic intensity depends not only on polarity and average refractive index, but on phase matching as well. The second harmonic wave must be kept in phase with the fundamental to radiate efficiently. In birefringent crystals this is accomplished by balancing the dispersion with birefringence so that waves of frequency ω and 2ω travel with the same velocity.

The refractive indices of kaolinite, dickite and nacrite are nearly identical with an average refractive index of 1.56 and very small birefringence, less than

0.006. Extrapolating the measured refractive indices to 1 μm gives a dispersion of about 0.015 between the fundamental (wavelength 1 μm) and second harmonic (wavelength 0.5 μm). The dispersion is not large, but exceeds the maximum birefringence by more than a factor of two. It is therefore impossible to balance birefringence against dispersion to produce phase matching.

Another reason for the small SHG signal of clay minerals is the small particle size. Clay mineral crystals are seldom larger than 1 μm, which is a factor of ten smaller than the SHG coherence length d_c. The coherence length refers to the phase difference between the fundamental and harmonic waves. The quantity d_c is defined as $\lambda/4(n_{2\omega}-n_{\omega})$, where λ is the wavelength of the fundamental, n_{ω} is the refractive index of the sample at the fundamental angular frequency ω, and $n_{2\omega}$ is the refractive index for the second harmonic. The coherence length for kaolinite family minerals is approximately 20 μm.

The dependence of SHG intensity on particle size has been studied by Kurtz and Perry (1968). Measurements were made on zincite (ZnO) and quartz (SiO_2), which, like the clays, are not phase-matchable. The second harmonic intensity is a maximum when the particle size is close to the average coherence length d_c. For smaller particles, the intensity decreases with size, dropping off to less than 10% of the peak signal when the particle size is ten times smaller than d_c.

Particle size appears to be an important factor governing the SHG intensity from clays as well. In Figure 3 harmonic intensities from six clay specimens are plotted as a function of particle size, as determined from electron microscope photographs. The plot shows considerable scatter but follows the same trend reported for quartz. The similarity to quartz is perhaps not surprising since the refractive indices, birefringence, and dispersion are about the same.

Some of the scatter in the correlation between particle size and SHG intensity shown in Figure 3 may be due to twinning. Mansfield and Bailey (1972) have recently described twins and pseudotwins in kaolinite. Twinning is expected to lower the harmonic intensity since it changes the sign of some nonlinear optic coefficients, thereby decreasing the effective particle size.

The preliminary SHG results on clay appear to be of sufficient interest to warrant further investigation, although a number of unanswered questions remain: Is the SHG signal a reliable indication of crystallite size and perfection? Are there significant variations for clays from different localities and from different geological origins? What modifications of the experiment are required to optimize SHG signals for fine-grained silicates? Will dispersion of the powder in index-matching liquids and Q-switching of the laser increase the intensities appreciably without damaging the specimens? Kaolinite crystallites are often arranged in "books" of parallel platelets. Are all the platelets arranged in a polar manner, or are some reversed in position? Are there preferred orientation effects similar to those observed in powder X-ray diffraction? What is the effect of adsorbed liquids on the SHG intensity? Is the arrangement of water molecules between layers polar or nonpolar? Micas, chlorites, and some other layer silicate families have both centric and acentric polytypes in which the layers are stacked differently. Will the SHG test provide a reliable method of identifying acentric polytypes?

If the factors governing second harmonic intensity can be controlled and understood, the test may prove to be useful in characterizing fine-grained minerals. In any case, the experiments on clay demonstrate the superiority of the SHG method over other physical tests for acentricity.

Acknowledgements. This work was sponsored by the Army Office of Research and Development (DAA 29-76-G-0145) and by the National Science Foundation (GH-34547). We also wish to thank our colleagues at the Materials Research Laboratory for their advice and assistance.

References

Franken, P.A., Hill, A.E., Peters, C.W., Weinreich, G.: Generation of Optical Harmonics. Phys. Rev. Lett. 7, 118–119 (1961)

Kurtz, S.K., Dougherty, J.P.: Methods for the Detection of Acentricity in Solids. In: Systematic Materials Analysis, Vol. IV: Richardson, J.H. and Peterson, R.V. (eds.). New York: Academic Press (in press)

Kurtz, S.K., Perry, T.T.: A Powder Technique for the Evaluation of Nonlinear Optical Materials. J. Appl. Phys. 39, 3798–3813 (1968)

Mansfield, C.F., Bailey, S.W.: Twins and Pseudotwin Intergrowths in Kaolinite. Am. Mineral. 57, 411–425 (1972)

Received March 18, 1977

Appendix 5

Second Harmonic Generation In Antiferroelectric PZT

SECOND HARMONIC GENERATION IN ANTIFERROELECTRIC PZT

M.K. Nelson, W.A. Schulze and R.E. Newnham

Materials Research Laboratory
The Pennsylvania State University
University Park, Pennsylvania 16802

INTRODUCTION

The structure of $PbZrO_3$ has been continually questioned since its first misidentification as a ferroelectric in 1950 (1). The antiferroelectric nature of lead zirconate was conclusively proven by Sawaguchi in 1953 (2). The structural determination was begun by x-ray diffraction which demonstrated antipolar shifts of the Pb ions in the a-b plane of an orthorhombic structure (3). This work was supplemented by single crystal x-ray and powder neutron diffraction. Analysis of the diffraction data was refined towards two structures, a centric and an acentric (polar) space group (4). The conclusion was that the structure was acentric and polar with oxygen atoms having an irreversible distortion resulting in a polar moment near that of $BaTiO_3$. This decision towards a polar structure may have been strongly influenced by the earlier report of piezoelectricity in $PbZrO_3$ by Roberts (5). The evidence of polarization was neither reproduced by pyroelectric measurements on ceramic (6) or reproduced by both piezoelectric and pyroelectric tests on single crystals (7). More recent work (8) using x-ray diffraction has indicated that the structure may be acentric but not polar.

At least part of the structural controversy results from the inability of x-ray techniques to determine acentricity. This study will use a relatively new technique, SHG, which has proven extremely sensitive to structural acentricity. Second harmonic generation from laser light, SHG, occurs when acentrically bounded valence electrons are exposed to the intense electric

field of a laser. A full explanation of this technique is given in the papers by Kurtz (9,10,11).

The approach used in this study is to compare the SHG response of $PbZrO_3$ to that of PZT's with known antiferroelectric (AF), ferroelectric (FE), and paraelectric (PE) phases. Figure 1 is a section of the PZT phase diagram and illustrates the comparative measurement. A 2% Ti addition allows stable regions of all three phases, while 10% Ti has a FE phase stable to room temperature. In this way the generation levels of a strongly polar and a centric phase could be studied in the same sample and compared to the generation of the unknown AF phase.

PREPARATION

Samples were prepared with 0 to 10% Ti. The method was a coprecipitation technique described by Biggers (12) and is reported to have superior homogeneity and purity compared to the conventional mixed oxide processes.

SHG intensities were measured while the sample was being heated or cooled by 2-4°C/min. The regional levels recorded are the summation for the total laser pulse and are relative to the equipment utilized. Intensities are related to a standard sample of high-purity $BaTiO_3$ ceramic.

Dielectric measurements were made on cooling at 2°C/min and consistently reproduced the peak permittivity within 1°C.

RESULTS

Figure 2 illustrates the dielectric anomalies resulting from the phase transition in PZT. The shoulders have been shown (2) to occur at the AF-FE transition and the maxima at the FE-PE transition.

Figure 3 illustrates the same transitions as interpreted by SHG. In this case the transitions are viewed by the large change in the generation

coefficients and an arbitrary level of intensity must be assigned to determine the temperature of transition. The transitions as determined by SHG and capacitance measurements are summarized in Figure 1.

Figure 4 shows the compositional dependence of the maximum SHG intensity. The similarity of all compositions indicates that the amount of Ti has only a weak effect on the generation coefficients. The closeness of the intensity of $PbZrO_3$ to the known ferroelectrics suggests that the FE phase exists in both heating and cooling.

Figure 5 shows the relation between the room temperature intensities for both FE and AF compositions. On this scale $BaTiO_3$ ceramic would have an intensity of about 400, which is similar to the PZT intensities and about two orders above the reference level of quartz. Quartz is a nonpolar-noncentric standard that is 2 to 3 orders above the level attributed to a working zero point intensity. The AF phases fall about 1.5 orders below that of quartz.

CONCLUSIONS

$PbZrO_3$ exhibits SHG intensities at the same levels as the ferroelectrics on both heating and cooling. This strongly suggests that the high-purity ceramic in this study has a narrow but stable FE phase region independent of thermal history.

The room temperature SHG intensities for the AF material are 3 orders of magnitude below the FE phase and 1.5 orders below nonpolar quartz. This evidence does not predict, but it strongly suggests, that the structure of AF $PbZrO_3$ is not polar but most likely is acentric.

REFERENCES

1. Roberts, S., "Dielectric Properties of Lead Zirconate and Barium-Lead Zirconate," J. Amer. Ceram. Soc. 33, 63-66 (1950).
2. Sawaguchi, E., "Ferroelectricity vs Antiferroelectricity in the Solid Solutions of $PbZrO_3$ and $PbTiO_3$," J. Phys. Soc. Japan 8, 615-629 (1953).
3. Sawaguchi, E., H. Maniwa and S. Hoshino, "Antiferroelectric Structure of Lead Zirconate," Phys. Rev. 83, 1078 (1951).
4. Jona, F., G. Shirane, F. Mazzi and R. Pepinsky, "X-Ray and Neutron Diffraction Studies of Antiferroelectric Lead Zirconate, "$bZrO_3$," Phys. Rev. 105, 849-856 (1957).
5. Roberts, S., "Piezoelectric Effect in Lead Zirconate," Phys. Rev. 83, 1078 (1951).
6. Shirane, G. et al., "Dielectric Properties of Lead Zirconate," Phys. Rev. 84, 476-479 (1951).
7. Scott, B.A. and G. Burns, "Crystal Growth and Observation of the Ferroelectric Phase of $PbZrO_3$," J. Amer. Ceram. Soc. 55, 331-333 (1972).
8. Whatmore, R., Private communication.
9. Kurtz, S.K. and T.T. Perry, "A Powder Technique for the Evaluation of Nonlinear Optical Materials," J. Appl. Phys. 39(8), 3798-3813 (1963).
10. Bergman, J.G. and S.K. Kurtz, "Nonlinear Optical Materials," Mater. Sci. Eng. 5, 235-250 (1969/70).
11. Dougherty, J.P. and S.K. Kurtz, "A Second Harmonic Analyzer for the Detection of Non-Centrosymmetry," J. Appl. Cryst. 9, 145-158 (1976).
12. Biggers, J.V. and S. Venkataramani, "Preparation and Reactivity of Lead Zirconate-Titanate Solid Solutions Produced by Precipitation from Aqueous Solutions," Mat. Res. Bull. 13, 717-722 (1978).

LIST OF FIGURES

1. Portion of the PZT phase diagram.

2. Relative permittivity for PZT compositions, where the number is the mole % Ti.

3. SHG intensity versus temperature.

4. Peak SHG intensity as a function of composition.

5. SHG intensity at room temperature as a function of composition.

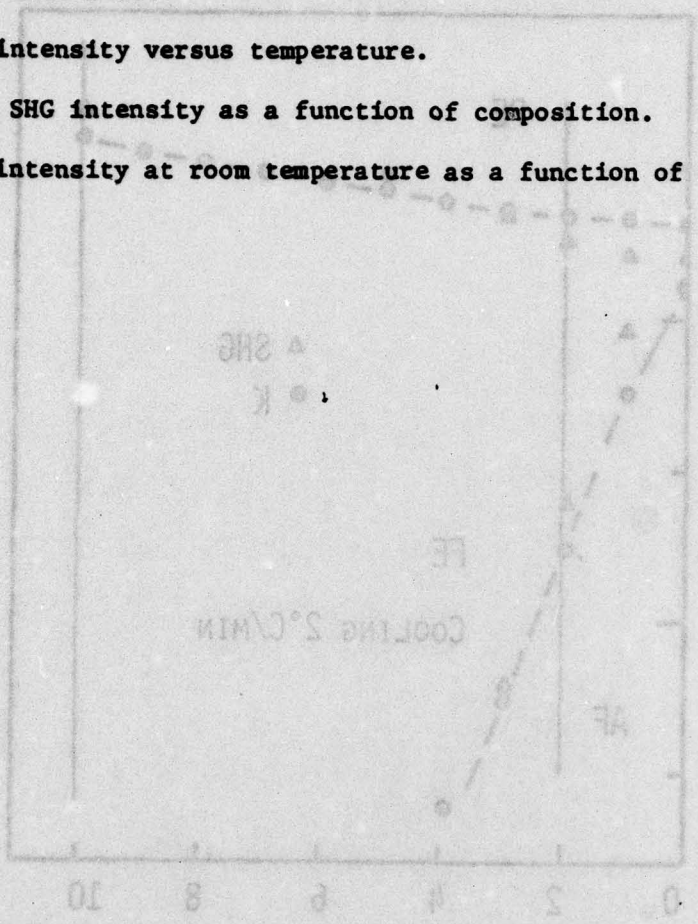

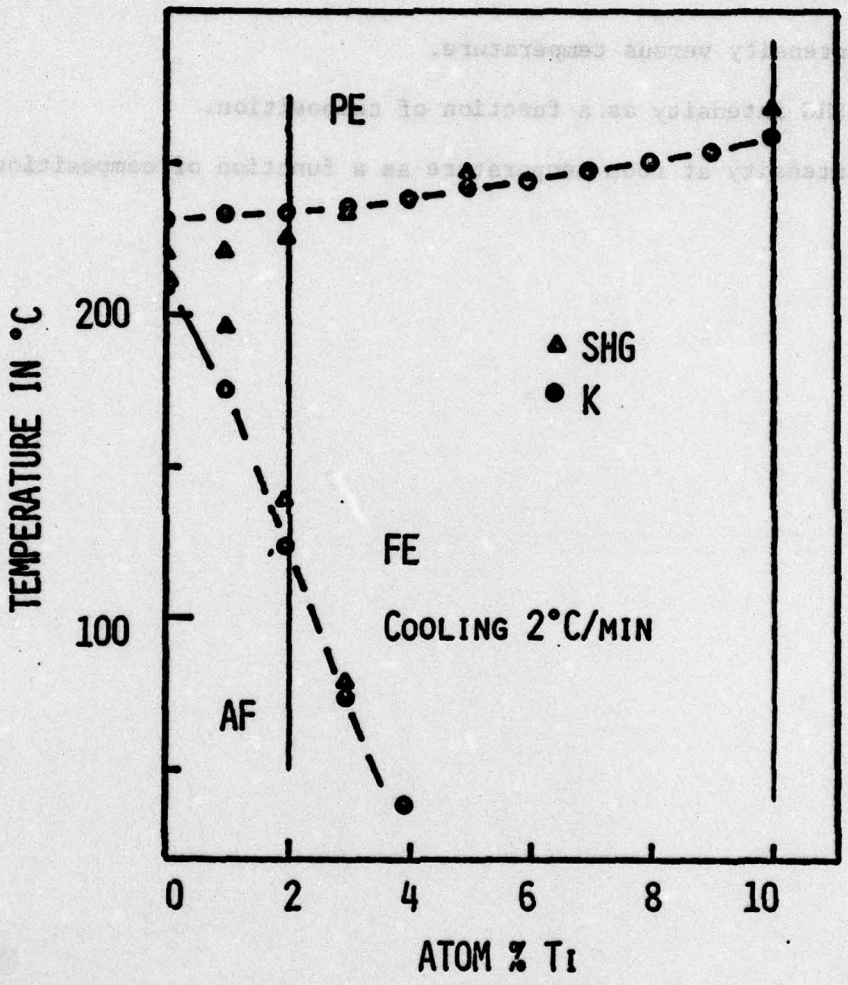
PE
200
100
TEMPERATURE IN °C
SHG
K
FE
COOLING 2°C/MIN
AF
0
2
4
6
8
10
ATOM % Ti

Figure 1

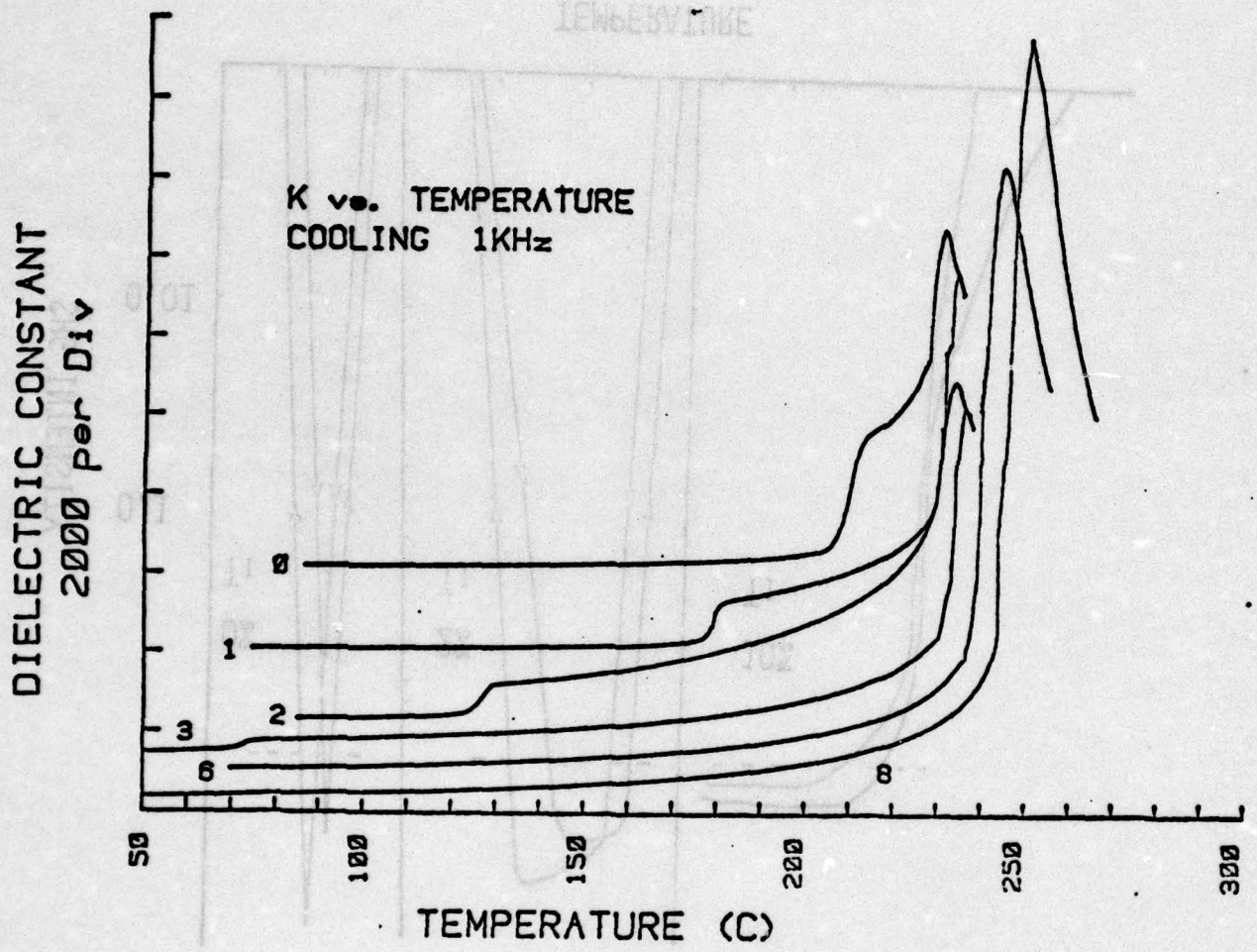
K vs. TEMPERATURE
COOLING 1KHz
DIELECTRIC CONSTANT
2000 per Div
0
1
2
3
6
8
50
100
150
200
250
300
TEMPERATURE (C)

Figure 2

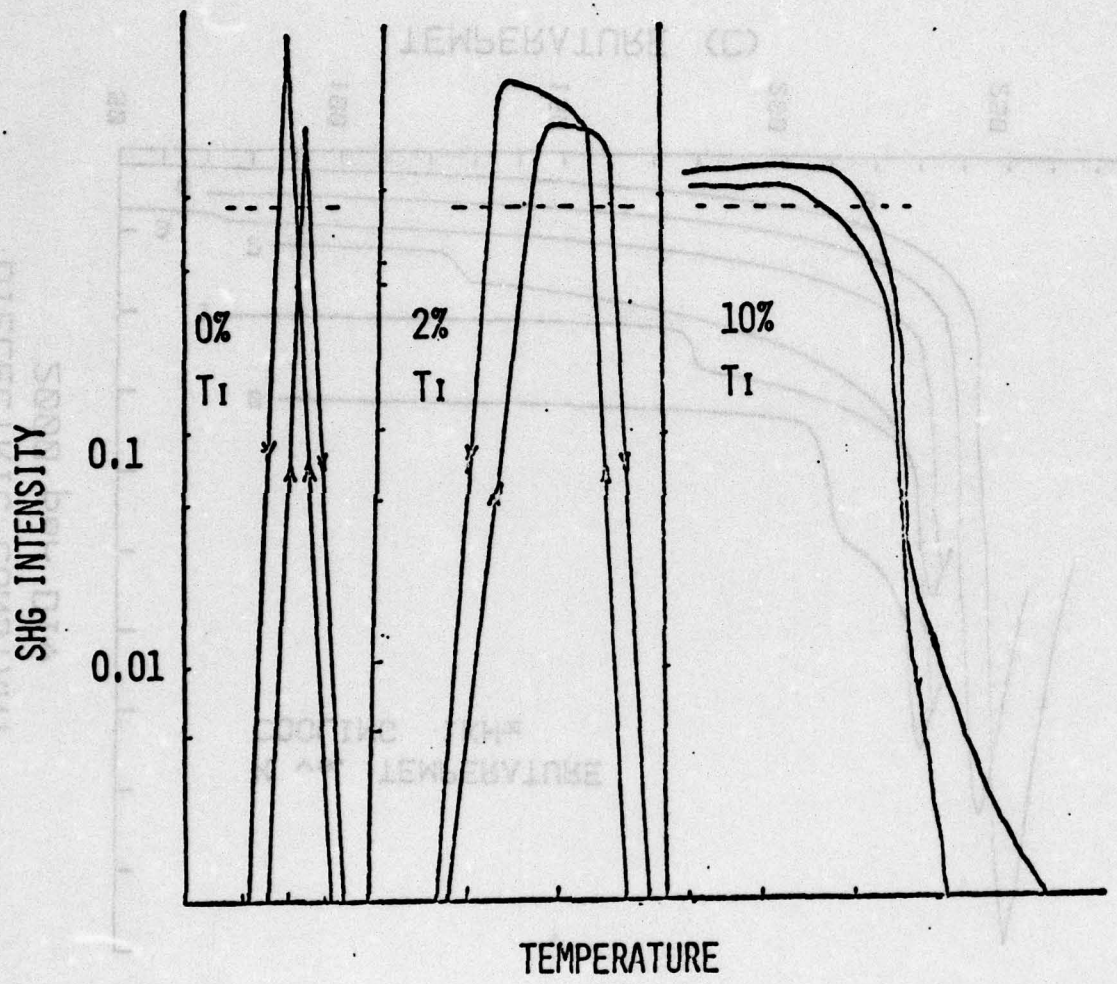

Figure 3

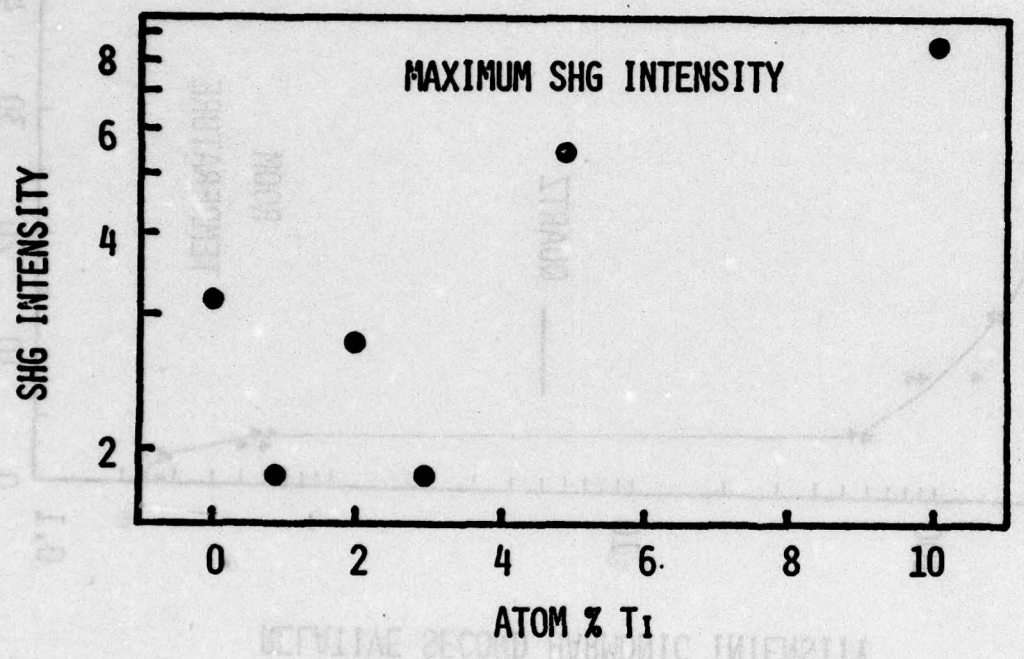

Figure 4

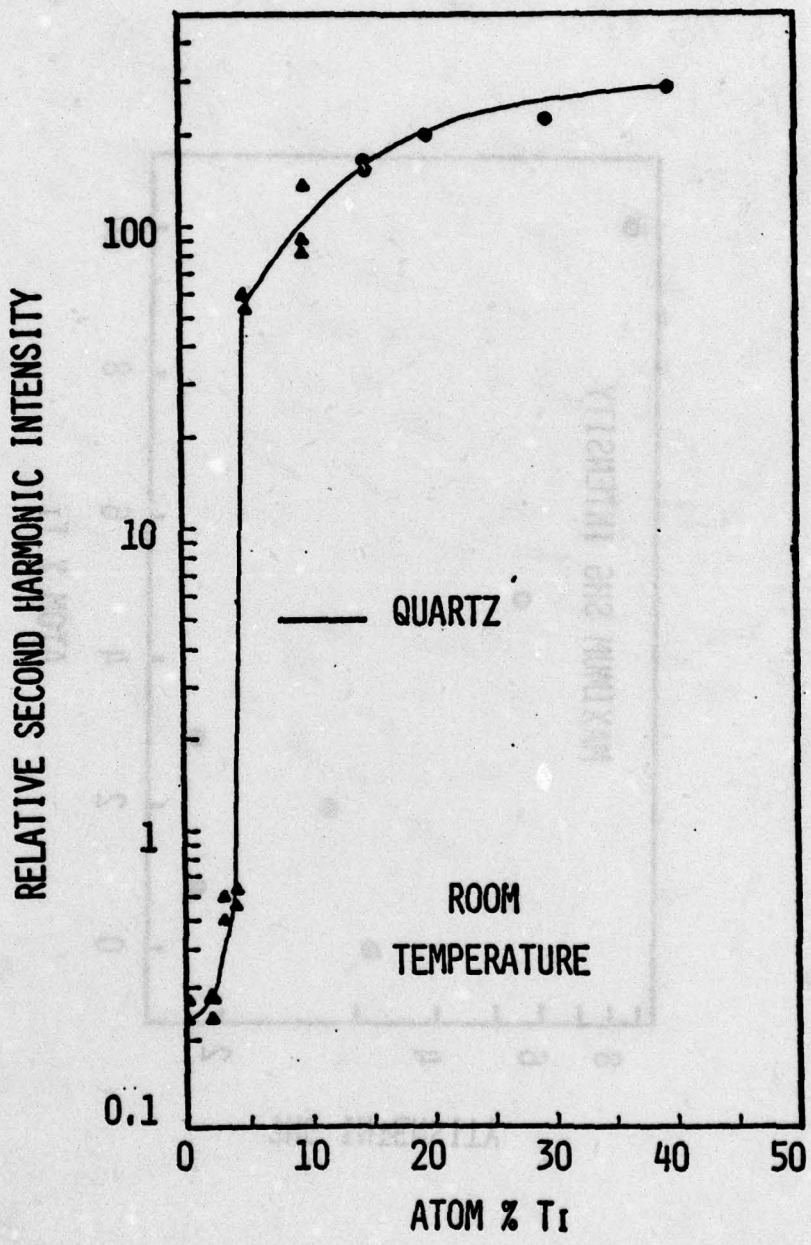
RELATIVE SECOND HARMONIC INTENSITY
100
10
1
0.1
QUARTZ
ROOM
TEMPERATURE
0
10
20
30
40
50
ATOM % Ti

Figure 5